CHAPTER 3

MODEL AND SABOT DESIGN AND LAUNCHING TECHNIQUES

by

Charles E.DeRose and Peter F.Intrieri

NASA-Ames Research Center

MODEL AND SABOT DESIGN AND LAUNCHING TECHNIQUES

Charles E.DeRose and Peter F.Intrieri

3.1 INTRODUCTION

In the preceding chapter, the operating principles and design of light-gas guns capable of accelerating projectiles to high velocities were discussed. Equally important to the ballistic range test is the projectile itself. The projectile usually consists of two parts, namely the part of interest in the test, the model, and its carrier in the gun, the sabot*. The model can be any body having the desired geometry and mass characteristics for which experimental data are required. The sabot alines and supports the model during the launching process.

It is necessary now to examine the design, construction and launching of the projectile. The designer's task is seldom an easy one, but represents the necessary first step in every successful ballistic range test. Many severe and often conflicting requirements must be satisfied before a successful design is achieved. The model must have the desired geometry, must withstand enormous launch accelerations, possess adequate aerodynamic stability (i.e., fly nose forward), and have the required mass and inertial characteristics dictated by test requirements. The sabot must also withstand the launch accelerations while supporting and protecting the model. Upon emerging from the gun it must also separate cleanly without imparting a large disturbance to the model and must not be allowed to hinder in any way the acquisition of data. It is seldom possible to achieve an *optimum* design which simultaneously satisfies all the imposed requirements. Rather, a successful combination of model and sabot is one which serves adequately to achieve the desired goals of the test. In a large number of cases this successful combination is not obtained through calculations alone, a development period of trial launches with some corrective redesign is often necessary to achieve the final useable configuration.

The purpose of this chapter is to discuss some of the basic principles of model and sabot design and to present and analyze typical examples of successful designs. It is hoped that the material presented will convey the state of the art and will offer the reader an appreciation of the problems involved and possible solutions to these problems. The chapter proceeds as follows: first, a general discussion of the problems that direct the initial design will be presented. A truly general discussion here is difficult because of the individual nature of each test and facility combination. However, the basic problems can be outlined to illustrate how the resulting constraints dictate the design. Next, detailed calculations pertaining to the design of a particular configuration (a 10^{o} half-angle cone) are presented to illustrate specifically the types of calculations performed in an actual model design. This particular example was chosen because most of the critical problems which can confront the designer are present, i.e., many conflicting requirements regarding model size, density, and inertia which require simultaneous solution, a relatively fragile model, high launch accelerations, complex sabot, heat protecting the model during flight, etc. The next two sections examine a number of actual designs of a variety of models and sabots which have been launched successfully at both low and high speeds. Here, the emphasis is on a detailed pictorial presentation where important features of individual designs are pointed out and discussed. Since the constraints on model design are usually more numerous and more severe for tests where the aerodynamic stability characteristics of the configuration are to be measured, the examples discussed are principally of this type. The next section is devoted to the subject of model measurement techniques. In this section, some of the methods used to determine a model's linear dimensions, weight, center-of-gravity position, moments of inertia and surface finish are discussed. The following section describes some of the auxiliary equipment used to separate the sabot from the model. These devices, while not directly a part of the design of models and sabots, are often required for successful testing, that is for example, to prevent sabot parts from entering the test area and to facilitate launching models in tests requiring low static pressure and other special situations. The chapter ends with a brief discussion of some of the techniques and equipment used in proof testing, that period of trial launches which precedes the use of the model for testing.

3.2 GENERAL DESIGN PROBLEMS

The design of particular models and sabots for ballistic-range tests is to some degree iterative. The constraints imposed by gun size, facility length, limits of operating pressure, number of photographic stations, and several lesser considerations determine how well the required data can be obtained in the desired flight regime. Usually, the design cycle is initiated by assuming an initial design based on prior experience which is then modified progressively as a result of various calculations.

---

* The word sabot is a French word which means wooden shoe (worn in various European countries). As used by ballisticians, it denotes the carrier or support used to launch various aerodynamic shapes and sub-caliber projectiles.

3.2.1 Initial Design Requirements

3.2.1.1 Design Conditions Imposed by Test Requirements

In tests where the aerodynamic coefficients governing the flight of a given configuration are to be measured, the mass and inertial characteristics of the model will have to be adjusted to meet both the velocity and density requirements of the test and the accuracy capabilities of the facility. If drag coefficient is to be determined, then the deceleration of the model must be large enough to be measured accurately, but not so large that it significantly alters the flight conditions*. Measurements of static stability, dynamic stability, and lift are possible only if there is sufficient definition of the model's pitching and swerving motion. In general, this requires that the wavelength of the pitching oscillations be less than two-thirds the length of the test section and that the swerve displacement be at least 20 to 30 times the measurement accuracy of the facility. To obtain the desired wavelength of oscillation, the model's size, moment of inertia, and center of gravity must be adjusted with respect to the free-stream density.

In tests aimed at studying the flow field around a model (such as, for example, boundary-layer transition), a primary design consideration is that of controlling the surface finish. Of course, these models must also be aerodynamically stable and capable of being flown at the desired flight attitude and velocity. Models for use in impact or flow-field radiation studies will be designed with the primary emphasis on shape, mass, and model material. A large amount of aerodynamic stability may have to be provided for these models since model attitude must be closely controlled in many of these tests; however, velocity changes during the flight are not usually a controlling factor.

The required velocity and Reynolds number of the tests put further constraints on model mass, dictate limits for model size, and narrow the choice of construction materials and assembly techniques. High velocity, in particular, causes the most problems in model design. In addition to extremely high accelerations that must be tolerated, heat-protective surfaces must sometimes be provided to keep the models from burning. In these tests a relatively simple design, that is, for example, solid homogeneous models constructed of high strength-to-weight ratio materials will usually afford the greatest assurance of success. Models for low speed tests generally offer a much wider choice of materials and can often be constructed of easy to machine sub-parts.

3.2.1.2 Design Conditions Imposed by the Facility

The facility to be used is the next important factor in model design. The length of the facility determines the amount of deceleration required for accurate drag measurements and puts boundaries on the wavelength of pitching oscillations. The density capability of the facility together with the velocity and Reynolds number desired may dictate the model size and hence the level of aerodynamic forces and accelerations that must be withstood. A facility which has a wide range of density capability allows greater flexibility in the design. The number of observation stations available, together with the precision with which the required measurements can be made, serve to establish limits for model deceleration and number of pitching and swerving oscillations. (To define the pitching and swerving oscillations of the model, it is desirable to have at least five observations per cycle of motion.)

Thus we see that the test objectives and facility can impose harsh requirements on the design of a ballistic model. We have not attempted to quantitatively define the design parameters involved, nor have we indicated specific solutions for satisfying the requirements; this will be done in Section 3.3 where we examine the design of a particular configuration for use at particular test conditions. However, it is clear at this point that most designs will result from a careful balance of numerous requirements, which in many instances are conflicting.

3.2.2 Structural Design Requirements for Model and Sabot

3.2.2.1 Model Considerations

One of the major problems in designing models and sabots is providing sufficient strength to survive the launching loads. The customary design procedure is to first calculate the constant acceleration in the gun (ideal operation) which would yield the desired velocity, given the length of the launch tube and the flight velocity desired. The appropriate equation is

$$A_{\text{const.}} = \frac{1}{2} \frac{V^2_{\text{muzzle}}}{l_{\text{launch tube}}} . \tag{3.1}$$

A factor which represents the ratio of the peak acceleration to this constant acceleration is then applied to estimate the maximum acceleration which will be experienced. This factor is usually determined from prior acceleration measurements in the gun (by microwave measurements during calibration of the gun for example) or from breech pressure histories in powder gas guns. This peak acceleration factor, is, of course, dependent on the type of gun, the muzzle velocity, and weight of the projectile; however, a good approximation is that it will be between 3 and 5.

---

* Changes in the flight conditions, that is, for example, Mach number, Reynolds number, are detrimental only if the desired aerodynamic coefficients vary with these changing conditions. However, this information is usually not known beforehand and so near-constant conditions during the flight are desirable.

Thus knowing the peak acceleration, a stress analysis is applied to critical sections of the model. It is assumed that the load across any section is that required to accelerate all the mass ahead of that section. Thus the stress analysis is fundamentally treated as a static loading; dynamic effects are very difficult to estimate and so are not usually considered in the initial design. Buckling of a particular section of the model may, however, be investigated and if a failure of this type is indicated it can be countered by thickening the walls (if possible) or by additional sabot support in this region.

It should be noted that although this structural analysis seems oversimplified, it has generally not been necessary to make it more complete. Instead it has been found that experience, plus a small number of trial or development launches (proof testing), can lead to successful designs. This in a sense is fortunate since the true nature of the loads imposed on the model during launch and the material's resistance to high-strain-rate stressing are not conclusively known. Exceptions to this procedure may arise when launchings are attempted at the highest possible velocities. Recently, attempts have been made by some experimenters to study theoretically the dynamic stress loading within very simple models and sabots[3.1]. The procedures are very complicated, however, and hence require a considerable investment of time, as well as access to electronic computers. Continuing research in this area of complete dynamic analysis is highly desirable and may in years to come prove a boon to the model designer.

Both the strength requirements and the model weight influence the choice of model material. A compromise to meet both requirements can sometimes be made by using two or more different materials in the construction or by hollowing a homogeneous model. Materials of high strength-to-weight ratio are usually of greatest advantage. Aluminum, magnesium, titanium, and high strength alloy steels are commonly used metals, while polycarbonate, polyamide, and polyethylene plastics are often chosen for sabots as well as for models. Table 3.1 shows the physical characteristics for some of the materials commonly used for ballistic models and sabots. Material cost is usually not an important factor in the selection since the quantity used in model construction is small. Machineability of the material, however, should be a consideration since accurate reproduction of the models is very important.

3.2.2.2 Sabot Considerations

As stated earlier the sabot is the supporting structure which is necessary to launch all sub-caliber models. The sabot alines the model in the gun, prevents model contact with the launch tube walls, and separates the model from the driving gases. It is frequently necessary to use models that are structurally weak relative to the predicted launch loads. In these cases, the sabot has been utilized to provide the necessary support for the weak sections. In fact, use of sabots which completely enclose the model has enabled successful launching of models which theoretically were too weak by factors of two or more. The use of the completely enclosing sabot, or a sabot that supports the internal structure of the model, extends the velocity capability of the model, but compromises the release process; this problem will be discussed in the next section.

Since the sabot must also withstand the accelerations during launch, the same type of stress analysis discussed previously in relation to the models is also usually applied to critical sections of the sabot. More specific discussion of these critical sabot sections and types of structural failure which can occur is given in Sections 3.3.2 and 3.4.

3.2.3 Design Considerations for Separation of Model From Sabot

While it is necessary for the sabot to support the model, seal off the driver gases, and keep the model alined and away from the launch tube walls, it is equally necessary to have the sabot separate from the model with minimum disturbance. The sabot, upon release of the model, should then veer away from the flight path of the model and not interfere with the acquisition of data (i.e., continue down range and trigger light sources in the observation stations which could cause double images on, and/or overexpose the photographic film, radiate light which could also blacken the film, follow the model too closely which could affect the wake flow and in turn affect the air pressure on the model base, damage parts of the instrumented test section such as vacuum lines, air lines, windows, measuring equipment, etc.). This separation of the sabot from the model is fully as important to the success of the test as protecting the model in the gun. These separation requirements lead toward a minimal, light-weight structure which generally conflicts with the requirement of maximum model support. The resulting compromise is usually a sensitive one and is frequently resolved only by proof firings.

3.2.3.1 Sabot Separating Forces

The way in which a sabot is designed to achieve a clean separation from the model upon emerging from the gun is fairly straightforward once one understands the forces available to accomplish the separation. Five types of separating force commonly used in ballistic range testing are: aerodynamic, propellant gas, internal elastic, centrifugal, and external mechanical.

Aerodynamic forces are most commonly used to separate segments of the sabot from the model. Pressure forces, acting on the beveled front face and/or hollow front section of the sabot pieces, force the pieces radially outward away from the model. Aerodynamic forces are also employed to achieve axial separation between a sabot base and the model. This method requires both a reasonably high air density and light-weight sabot segments (relative to model weight) to obtain good separation.

For sabot designs in which the front face cannot be shaped to utilize aerodynamic forces, an alternative is to use the pressure force of the propellant gas. Usually, in such cases, the sabot is split in two or more

pieces with a hole or cavity machined in from the base at the interfaces of base pieces and also fingers. This hole is filled with the high pressure propelling gas while the model and sabot are being accelerated in the gun. Upon leaving the launch tube, this high internal pressure forces these sabot pieces apart, away from the model. This same configuration can be used with a metal spring to produce the separating force (here the response time of the spring relative to the flight duration must be very short), but the gas pressure method is simpler and much more powerful.

Similar to the above design, internal elastic forces in the sabot material can also be used to provide a separating force. The segmented sabot is made slightly oversize and compressed when loaded into the launch tube. Upon leaving the barrel, the rebound of the material causes the segments to separate. This latter method is not as positive as the one employing the internal gas pressure, but may be of advantage when positive gas sealing is required.

The method of using centrifugal forces to separate sabot segments is extremely powerful, and does not rely on any internal or external pressure forces. However, its use is limited to those tests in which a high model roll rate is either desired, or is not detrimental to the test. This method is also dependent on the availability of a rifled launch tube. In the case of modern, light-gas guns, a rifled tube can be very expensive and difficult to obtain.

With some configurations, it is impossible to use the separating forces previously mentioned. In these cases, a mechanically-applied decelerating and deflecting force must be employed. This force is usually provided by a muzzle constrictor or sabot stripping plate. A retarding force may thus be applied to a full bore diameter sabot (base) to achieve an axial separation between it and a subcaliber model. After the axial separation is achieved, a deflecting ramp can be used to divert the sabot away from the flight path of the model. A further discussion of this method will be presented in Section 3.7.

3.2.3.2 Separation Dynamics

After separation of the sabot segments from the model is achieved, some attention must be placed on the flight dynamics of the pieces. Hopefully, the pieces can be made light and of high drag shapes so that their deceleration is greater than that of the model. If this can be achieved, then the axial separation of model from sabot pieces can prevent any further interference. Heavy sabot segments which decelerate less than the model will usually have to be trapped by a sabot stripper – a plate with a hole on gun centerline large enough for only the model. Additional features of mechanical strippers and deflectors will be discussed in Section 3.7.

3.3 TYPICAL EXAMPLE OF DESIGN PROCEDURE

In the preceding section we discussed in general terms the types of problems associated with the design of models and sabots. Let us now examine a specific example to illustrate the actual design procedure in more detail. In doing this, we will describe the types of calculations that are made and give actual numbers to enhance the previous general statements.

The most demanding set of constraints is usually that imposed by aerodynamic stability tests, since all the constraints concerning model deformation and disturbance at launch are present together with others pertaining to scale, material, moments of inertia, and center-of-gravity location. Hence, let us consider the design of a 10^{0} half-angle cone to be tested in a given flight regime for the purpose of measuring drag, static and dynamic stability and lift. The Mach number and Reynolds number range of the tests along with a description of the facility in which the tests are to be conducted are given in Table 3.2.

3.3.1 Model Design

If, first, it is assumed that the model will be of maximum size, compatible with the gun, i.e., 1.27 cm diameter, then the free-stream pressures will be:

$$P_{\infty} = 0.022 \text{ atm for } R_{e\infty} = 100{,}000$$

$$P_{\infty} = 0.22 \text{ atm for } R_{e\infty} = 1{,}000{,}000 \, ,$$

given $R_{e\infty} = \rho_{\infty} V_{\infty} d/\mu_{\infty}$, $\rho_{\infty} = P_{\infty}/RT_{\infty}$, $V_{\infty} = 5.2$ km/sec , and $T_{\infty} = 290^{0}$ K . It can be seen in Table 3.2 that these pressures are within the pressure capability of the facility, hence, the desired Reynolds numbers can be obtained in this facility with this size model.

For drag measurements, the deceleration must lie between some lower limit of measurability (Chapter 7) and an upper limit imposed by the requirement that test conditions do not vary significantly along the flight path (see footnote page 3-2). For these tests, it is desired to keep the change in Mach number to the order of 0.2.

A commonly used measure of the effect of drag on the trajectory is the distance decrement which is the difference in distance traveled, in a given time, between the actual model and a model with zero deceleration. For small changes in velocity, this distance decrement is given by

$$X_D = \frac{1}{2} A t^2 = \frac{1}{2} \left[\frac{C_D \frac{1}{2} \rho_{\infty} V_{\infty}^2 S}{m} \right] t^2 \, , \qquad (3.2)$$

where

A = deceleration, m/sec^2

C_D = drag coefficient

ρ_∞ = free stream density, kg/m^3

V_∞ = velocity, m/sec

m = model mass, kg

t = time, sec

S = model reference area, $\pi d^2/4$, m^2

d = model diameter, m.

The distance decrement may also be written

$$X_D = \frac{1}{2}\left[\frac{\Delta V_\infty}{t}\right] t^2 = \frac{1}{2}[\Delta V_\infty] t \ . \tag{3.3}$$

With $\Delta V_\infty = 0.2\ a_\infty = 0.2\ (344) = 68.8$ m/sec , and $t = l_{ts}/V_\infty = 23/5150 = 4.5 \times 10^{-3}$ sec (a_∞ is the speed of sound and l_{ts} is the length of test section), then the specified upper limit for the distance decrement for these tests would be

$$X_D = \frac{1}{2}[68.8][4.5 \times 10^{-3}] = 0.155 \text{ m} \sim 16 \text{ cm} \ . \tag{3.4}$$

The lower limit of X_D , necessary for accurate drag measurements, depends on the accuracy with which distance measurements could be made in the facility and is estimated to be about 2.5 cm for the facility assumed here. This corresponds to an accuracy of 0.13 mm in the measurements of model position in the shadowgraphs and a time measurement accuracy of 0.02×10^{-6} sec.

The effects of the principal model parameters on the distance decrement can be displayed by rearrangement of Equation (3.2). For this purpose, we may assume that velocity is constant for the flight. Then velocity and time can be eliminated from the equation in favor of distance.

$$X_D = \frac{1}{4}\frac{C_D \rho_\infty S}{m}[l_{ts}]^2 \ . \tag{3.5}$$

Equation (3.5) gives explicitly the sensitive dependence of drag-measuring accuracy with test section length. Further, since model mass (m) varies directly with $(\rho_m d^3)$, where ρ_m = model density , and S varies directly with d^2 , then

$$X_D \sim \frac{[C_D][\rho_\infty]}{[\rho_m][d]}[l_{ts}]^2 \ . \tag{3.6}$$

Equation (3.6) shows that the distance decrement varies inversely with model scale and model density, and directly with air density.

The minimum drag coefficient for this cone is estimated to be about 0.10. With this drag coefficient, a test section length of 23 meters, and a free stream air density 0.022 × standard atmospheric density (to satisfy the lower Reynolds number requirement), the model weight must be 1.8 grams for $X_D = 2.5$ cm and 0.28 gram for $X_D = 16$ cm . Thus, an acceptable weight for this model would lie between 0.28 and 1.8 grams. Since the model volume is about 1.5 cm^3, this would require (for a solid model) materials having densities around 1 gram/cc (plastics). Since the weight of the model must vary directly with the free stream pressure to keep the distance decrement constant (see Equation (3.6)), the model for testing at 0.22 atm must weigh between 2.8 grams and 18 grams. These weights call for model materials with densities of metals. For both regions of this test, it is advisable to keep the model weight toward the heavy limit because the drag coefficient increases sharply with angle of attack. For example, C_D at 10^o angle of attack is almost double that at 0^o. Thus, to avoid a large change in velocity during flights experiencing moderate angles of attack (necessary for measurement of lift), the model weight must be larger than the minimum values given above.

In the test, the static stability of the configuration (as measured by the moment-curve-slope, C_{m_α}) will be determined from the wavelength of the pitching oscillations given by the relation

$$-C_{m_\alpha} = \frac{8\pi^2 I_y}{\lambda^2 \rho_\infty S d} \ , \tag{3.7}$$

where

I_y = moment of inertia about y-axis, $kg\text{-}m^2$

λ = wavelength of pitching oscillations, m

d = model reference diameter, m.

To obtain accurate stability data (in particular, dynamic stability) 1½ to 2 cycles of motion are desired; i.e., the wavelength should lie between $\frac{2}{3} l_{ts}$ and $\frac{1}{2} l_{ts}$. The factors controlling the wavelength are given by Equation (3.7). Thus, in designing the model, C_{m_α} must be estimated, which requires knowing the position of the center of gravity. A homogeneous cone with a half angle of 10^o has its theoretical center-of-pressure location about 0.31h from the base and its center of gravity at 0.25h from the base. With this center-of-gravity position further aft of the center of pressure, the configuration is aerodynamically unstable. Hence, the center of gravity must be placed forward of the 0.31h position either by hollowing the base of the cone or by ballasting the nose. The former method is usually preferred with plastic models because the plastic will usually not be strong enough to support heavy materials at the tip. The latter method, however, is frequently used with metal models. Since the desired weights of the models have already indicated use of plastic materials at the low Reynolds numbers, the method of hollowing the base is chosen for these models.

With the base of the model machined out as shown in Figure 3.1, the center of gravity is moved forward to 0.35h from the base. The static stability derivative, C_{m_α}, computed using Newtonian theory for this center-of-gravity position is -0.21 per radian (based on d). If nylon is used as model material (ρ_m = 1.1 grams/cc), the model would weigh 0.91 gram (acceptable for drag measurements at the lower Reynolds numbers), and have a pitch moment of inertia of 6.1×10^{-8} kg-m^2, which would result in a pitching-motion wavelength of 21 meters at a free stream pressure of 0.022 atm. This wavelength is about $0.9 l_{ts}$, which is greater than the prescribed upper limit for λ, and hence, would not yield accurate stability data. The desired wavelength should be from 12 to 15 meters.

Equation (3.7) can be expanded and the terms rearranged to obtain

$$\lambda \sim \left[\frac{1}{\sqrt{(-C_{m_\alpha})}}\right]\left[\sqrt{\left(\frac{\rho_m}{\rho_\infty}\right)}\right][d] \quad . \tag{3.8}$$

It is seen from Equation (3.8) that reducing the model size is an effective way of reducing the wavelength. However, when the model size is reduced, the free-stream density must be proportionately increased to keep the Reynolds number constant; for a constant Reynolds number, the wavelength is proportional to $d^{3/2}$. These changes also increase the distance decrement in the drag analysis, so these limits must be rechecked. However a $\frac{2}{3}$ size model, base diameter of 0.84 cm, tested at 0.034 atm ($R_{e\infty}$ = 100,000) would have a wavelength of 12 meters (acceptable) and a distance decrement of 6.9 cm (also acceptable).

For measurements of dynamic stability, at least three well defined peaks in the pitching oscillations are necessary, which, for this facility, would require a wavelength of 16 meters or somewhat less. With the 0.84 cm diameter nylon model, we satisfy this requirement also.

To determine lift (as measured by the lift-curve slope, C_{L_α}), the displacement of the model's swerving motion about a mean line, Z_{swerve}, is measured. The appropriate equation is

$$Z_{swerve} = \frac{C_{L_\alpha} \alpha_{max} \rho_\infty S \lambda^2}{8\pi^2 m} \quad . \tag{3.9}$$

For a 0.84 cm diameter nylon model at 0.034 atm pressure, assuming a theoretical value of C_{L_α} = 1.78 per radian, and a maximum angle of attack, $\alpha_{max} = 10^o$, the maximum swerve displacement would be 0.5 cm. This amount of swerve should yield accurate results since the accuracy of these measurements in this facility is of the order of 0.13 mm or about 2½ percent of the maximum displacement. Equation (3.9) can be rearranged to obtain

$$Z_{swerve} \sim \frac{[C_{L_\alpha}][\alpha_{max}][d]}{[-C_{m_\alpha}]} \sim \frac{[\alpha_{max}][d]}{[\text{static margin}]} \quad , \tag{3.10}$$

where the static margin, for small angles of attack, may be written

$$\text{static margin} = \frac{x_{cg} - x_{cp}}{d} \approx -\frac{C_{m_\alpha}}{C_{L_\alpha}} \quad . \tag{3.11}$$

It can be seen from Equations (3.10) and (3.11) that the swerve depends only on the model size and the amplitude of pitching oscillation for a given static margin.

Since it was specified that data be obtained at Reynolds numbers from 100,000 to 1,000,000, models having different densities will be required. Using the basic model geometry shown in Figure 3.1 and the various scaling equations, the set of models of Table 3.3 can be formulated.

As can be seen in Table 3.3, three models, all the same size but of different materials, will cover the test range. The use of similar models but of different materials will usually result in low machining cost and good accuracy in reproduction. A single group of form tools can be used to machine all the models. Also, with the model size and geometry constant, a common sabot design can often be used.

The models just described will satisfy the test requirements but only if (1) they can be launched at the desired velocity without damage, and (2) if they survive the aerodynamic heating and pressure loading during the flight with no significant change in shape. To determine whether a structural failure of the model (and/or sabot) is likely to occur during launch, a simplified stress analysis is performed at critical sections in the model and sabot. This analysis involves calculation of the compressive stress at sections A-A and B-B (see Figure 3.2) and possibly at other intermediate sections. In these calculations the ultimate compressive strength

as determined from static tests is usually used as a criterion to predict model failure. The possible increase in strength due to rapid strain rates in the actual dynamic loading serves as an unknown safety factor. For the desired velocity of about 5 km/sec, a maximum acceleration of about 1×10^6 gravities occurs with the particular light gas gun to be used. At these conditions, the calculations indicate that the base (annulus) of the nylon model would fail in compression when the acceleration forces are applied only on the base, but that the steel and aluminum models would survive. However, it can be seen that if the plastic model is supported along its entire base area (internal cavity and base annulus) by means of an internal plug in addition to being supported externally along the skirt, much higher launch accelerations can be sustained. (As indicated in Figure 3.2, a fillet is used to alleviate stress concentration.) This example illustrates how sabot design can be used to overcome structural deficiencies in a model. Because plastics are much weaker than metals, the design of sabots for use with plastic models is more critical than for those used with metal models.

Other types of structural failures which might occur, particularly with the nylon model are: buckling of the thin skirt; bending or breaking off part of the model nose by convergence of stress waves in the tip or rarefaction waves produced within the model during the launch accelerations; and shearing off part of the model due to lateral accelerations developed by irregularities in the launch tube. These types of failures, however, are very difficult to investigate analytically; therefore, their occurrence is determined by trial launches. Here, again the importance of a good sabot design in achieving successful launches of fragile models can be demonstrated; in many cases it was found that complete encapsulation of plastic models within sabot "fingers" prevents these types of failures from occurring. Examples of plastic-cone models which used this type of sabot in actual tests will be presented later in this chapter.

In cases where hollowing the base of the model is not sufficient to move the center of gravity forward a desired amount, or where the nose of the model will burn because of high heating rates during the flight (the latter will probably occur for both the aluminum and steel models at the test conditions of this example), the designer will often use a bimetallic model such as the one shown in Figure 3.3. In cases where heating is not a problem, the important properties of the nose ballast material are that it has relatively high density, high strength-to-weight ratio, and is machinable. Sintered tungsten alloys are commonly used for this purpose. In tests where heating is important, metals which have very high melting temperatures (and also meet the other requirements just mentioned) such as tungsten, tantalum, and molybdenum are used. The problem of determining whether or not a material will burn during flight will be discussed in Section 3.5 where other solutions to this problem will also be discussed.

For the bimetallic model shown in Figure 3.3, it is again important that a simple stress analysis be made to insure that a structural failure does not occur at the joint of the two materials during launch. Stresses at the lower sections of the model will also increase due to the increased weight at the tip. Thus, the calculations of the compressive stress at sections A-A and B-B must be repeated. The design of the joint between the ballasting tip and the afterbody is critical. Considerations which can help prevent failure of this joint are to use fine threads for a screw attachment, and to achieve nearly zero clearance at both the base of the nose and the base of the screw so that the weight of the nose is distributed over the maximum available cross-sectional area. Other types of failures which have been known to occur and therefore should be examined analytically are: failure of the screw in tension or shear at section C-C or shearing of the screw threads of either material. Examples of several successful bimetallic model designs will be presented and discussed in Section 3.5.

3.3.2 Sabot Design

Several aspects concerning the design of sabots for the models of this example have already been implied in the previous discussion. The sabot shown in Figure 3.4 provides the internal pusher plug and complete encapsulation required for the plastic models, while the sabot for the homogeneous metal models (Fig.3.5) pushes only on the base annulus and uses shorter fingers.

A stress analysis is also required for the sabot to determine where failures might occur. Typical analyses performed are the following: compression at section D-D, bending along section E-E, and shearing along section F-F. These stress calculations are again based on the peak acceleration, or its equivalent, the peak gas pressure on the base of the sabot.

The front section of the sabot for the plastic model, by enclosing the model completely, acts to prevent buckling of the thin skirt and in addition supports the delicate tip. As shown, the front section of these sabots is split into four segments (fingers) to facilitate a cleaner separation from the model while shear pins, machined integral with the fingers, are provided to prevent differential axial movement of the segments during launch. The segments are separated aerodynamically by the pressure forces acting on the beveled front face. These four segments are usually machined from polycarbonate plastic (Lexan), a material chosen for its excellent strength and light weight. The base of the sabot could be either polycarbonate or polyethylene and is machined to fit the cavity of the model accurately. After the front segments have separated, the base piece being a full 1.27 cm diameter, decelerates behind the model in flight due to its higher drag. The base is not split into segments and so serves as a gas seal.

For the metal models, an aluminum insert is used in the plastic base to distribute the high stress under the thin base annulus of the model into the plastic. Because of the higher tip strength of the homogeneous metal models, complete encapsulation of the model in the sabot may not be necessary. Hence, an appreciable reduction in total projectile weight is achieved with consequent advantages in gun performance.

The models and sabots described in this section represent a configuration that has been successfully launched and tested. The final configurations, as used, were the hollow plastic and hollow bimetallic (tantalum nose, aluminum afterbody) models. The sabot shown in Figure 3.4 was the type used. The model shape in this example is simple, but the conditions of the test impose very critical requirements on the final design.

For models of more complicated geometry, the same general approach to design can be followed. Ordinarily however, the more complex shapes will be more difficult to launch without damage and so may be limited to lower speeds. The configurations that have been successfully launched are so varied that a complete comprehensive discussion would be impossible. As an example, Figure 3.6 shows the variety of models tested at only one laboratory. The approach in the next two sections will be to select a number of representative shapes and show how their design was directed.

3.4 MODELS AND SABOTS FOR LOW-SPEED TESTS

In the low-speed range, arbitrarily defined here to extend to 2000 meters/second (a velocity which is easily attainable using powder-gas guns), there exists a great deal of freedom in the type of model which can be tested and in the type of design and construction that can be used. For example, large models are feasible in this speed range because of the wide availability of large-bore guns. The advantage of large size permits the use of very intricate models with some degree of economy; and the low speed, with its low-acceleration loads, allows these frequently fragile models to be launched without damage. (Size however, must be compatible with facility length and pressure capability as was discussed in the example in Section 3.3)

To attain a successful design for model and sabot, even for this rather forgiving low-speed regime, one must first estimate the forces and stresses which will be applied to the model during launch and in some cases also during flight. The stress analysis for the more complex models must consider a number of additional failure modes. Consider the example of Figure 3.7.

For the model:

(a) Compression at the base.

(b) Shear at wing and tail root joints.

(c) Compression at body joints, especially between different materials.

(d) Column stability of body (determine whether supporting fingers are needed).

(e) Deformation of tail.

For the sabot:

(a) Bending along section AA (both stress level and deflections are important. Excessive deflection of base can distort rear fins or other thin sections.)

(b) Compression across section BB.

(c) Shear across section CC.

(d) Column stability of member L.

In addition to consideration of model strength, difficult design problems might be encountered in ballasting, obtaining the required model density, and in devising a sabot that will support the model during acceleration and release it cleanly with minimum disturbance. Let us examine some specific cases in which these problems were solved and successful designs were obtained.

3.4.1 Models Assembled from Individually-Machined Sub-Parts

Starting with models used for testing in the transonic to low-supersonic speed range (velocities up to about 500 m/sec), we will examine a series of models produced by assembling easy-to-machine sub-parts. Let us first consider two examples of models having wings and tails. Figure 3.8 shows an example of an airplane-like model tested at velocities up to 500 m/sec (Ref.3.2). The relatively low launching loads expected allowed the construction of this model to be kept simple and therefore economical. The model was constructed of four separate pieces, namely, a nose, body, wing and tail section which were pinned together. The body, wing, and tail section were 2024 aluminum. The nose was bronze to move the center of gravity forward for aerodynamic stability. To minimize the amount of bronze, the aft section of the body was hollowed out. The materials selected here were chosen merely on the basis of density, machinability and availability; strength of materials was only a secondary consideration, even for the aft section of the body which was hollow. The model size and weight were dictated by the facility used (an instrumented length of 20 meters at atmospheric pressure), the wavelength of oscillation in pitch (12 meters), and by the availability of a 7.6 cm diameter launch tube. The separate sections of this model were assembled using a press fit. The alinement of the nose and aft sections with the rest of the body was maintained by the long studs used for the press fit. In addition, steel pins were used to assure that the joints did not separate. Because the sections for the fins were quite thin, they were machined from a solid piece of aluminum, and so were integral with the cylindrical aft section of the body.

The sabot used to launch this model is shown in Figure 3.9 and consisted of a steel-faced, cast, hollow plastic cup with four foamed-plastic fingers. The sabot base was cast to allow inexpensive reproduction without resorting to repetitive machining of large diameter plastic stock. The plastic was reinforced with glass fiber to strengthen the crown. The hollow design was used to minimize weight so the sabot would decelerate behind the model after launch. The thin skirt also served as a gas seal. The steel plate cast in the front face of the

sabot was used to distribute the acceleration loads into the plastic. The sabot fingers were cut from very light, rigid-foam plastic and were used to aline the model initially for loading into the gun. The accelerating forces kept the model alined during the launch (the fingers probably collapsed during this initial part of the acceleration) and the model emerged from the muzzle essentially free of all restraint.

A slightly different design approach was used for the model shown in Figure 3.10. This configuration was used to study drag at transonic speeds. It was designed to be launched from a 7.6 cm diameter gun into air at one atmosphere pressure. Again, multiple-piece construction was used but in this case, the wing and tails were glued into slots cut in the body. A commercially available epoxy glue which had a thick non-running consistency worked well for this application. The design philosophy here was that the glue joint offered more restraint than pinned construction because of the extremely thin sections and large contact area inside the body. Steel was used for the wings and tails to obtain sufficient stiffness in these thin sections. A long brass nose was used with an aluminum body and a hollow magnesium aftersection to provide static aerodynamic stability; maximum stability was desired because of the requirement to measure drag at small angles of attack.

Because of this model's low drag and relatively heavy weight, a solid sabot base was used. The base was machined from nylon and a brass front face was used to distribute the load from the small diameter model base into the plastic. This simple sabot was possible because of the large difference in aerodynamic deceleration between model and sabot which assured quick axial separation. Foam plastic fingers were used with this model also, merely to keep the model alined during loading. This sabot offered nearly disturbance-free launches.

Both of the preceding models are examples of a potentially large group of multi-piece winged models that can be launched using simple sabots and temporary, weak, alinement fingers. This type of sabot arrangement offers the advantage of permitting the largest possible model for a given size gun (the wing span is limited by gun bore only) and the least chance of damage to the delicate wing and tail sections. The requirement that deceleration of the sabot base be much greater than that of the model is usually easily met with these slender winged bodies.

The sabots just discussed are examples of simple types which can be used to launch winged configurations. However, much more complex sabots must sometimes be used to launch very intricate and fragile models. One such example which gave consistently good results is shown in Figure 3.11 along with the model[3.3]. As shown in this figure, this sabot is made in four segments which are separated aerodynamically from the model by the high ram air pressure inside the cylinder when the sabot emerges from the muzzle. This separation process removes the segments from the flight path of the model. The long length of this sabot gives good alinement within the gun and supports the model well during launch. These cylindrical sabots are of course more costly than the simpler type shown in Figure 3.9, but their cost can be insignificant compared to that of the highly complex models they must launch.

Another low speed model and sabot combination is shown in Figure 3.12 (Ref.3.4). This model differs from those discussed previously in that it has very high drag and in addition had to be made very lightweight. These two factors combine to give the model a low ballistic coefficient (m/C_DS), which usually results in high deceleration. The model construction was dictated primarily by the desire to launch the configuration at a velocity of about 800 m/sec into still air at low static pressure (0.01 atmosphere). To afford maximum strength and light weight, the body, skirt (or drag ring), and upper struts were machined from a solid block of 2024 aluminum (a tape-controlled milling machine was used for this particular operation). The lower struts which would not experience high loading, were soldered in place after machining the rest of the model. The nose was made of bronze for ballast.

Because of the high-drag/low-weight characteristics of this model, of primary concern was the design of an appropriate sabot. To achieve minimum weight the sabot was cast in rigid polyurethane foam. To assure positive separation from the model, the sabot was forcibly decelerated by shearing off the outer wall material (approximately 0.05 cm thick) of the sabot at the muzzle of the gun. No alinement fingers were used here because of the natural, self-positioning characteristics of the skirt. The model base was fastened to the sabot with a small amount of wax, which kept the model alined until the launching loads were applied. The base of the model which experienced high loading during the launch was supported on a polycarbonate plastic pedestal, while the lightly loaded skirt was supported on the polyurethane foam. This was done to equalize the compressive strain at the two points to prevent distortion.

Figure 3.13 shows a model of the Apollo launch-escape configuration with its sabot[3.5]. The model consisted of three principal parts; namely, the tower, the music-wire supports, and the blunt-face capsule. The tower and capsule sections were constructed from 7075-T6 aluminum with tungsten-alloy ballasts; the struts were made of 1.5 mm music wire and were press fit into the base of the tower and capsule. The model was launched at speeds from 200 to 400 m/sec into air at one atmosphere using a 57 mm powder-gas gun.

The sabot was made of polyethylene to minimize weight and consisted of six pieces. The two-piece base had shear pins to prevent differential movement of the halves during launch. The four fingers were used here to aline the long front section of the model but not to support it; all compression was taken through the music-wire supports into the base*. This was done to eliminate possible interference between the fingers and the base of the tower section during the separation process. Separation of the fingers was initiated by aerodynamic forces acting on the beveled front faces.

---

* When fingers were not used slight misalinement of the model in the gun caused permanent bending of the music-wire supports.

All of the above models were launched using smooth-bore guns and so the model roll rates obtained were usually quite small. In cases where a high model roll rate is desired or where large centrifugal forces must be utilized to achieve positive sabot separation, rifled launch tubes are used[3.6,3.7]. Examples of models which were launched from a 37 mm diameter rifled, powder-gas gun to obtain high roll rates are shown in Figure 3.14. These models were used to measure the rolling moment developed by trailing-edge spoilers, (as shown, various size spoilers, were used)[3.6]. To achieve a low axial moment of inertia which in this case was necessary so the spoilers could produce a high roll acceleration, the body was constructed from relatively lightweight materials (i.e., aluminum with a hollow magnesium aft section). This bimetallic construction gave an aerodynamically stable configuration. The cruciform tails were made of steel to afford maximum stiffness and were silver soldered into slots cut in the aft section of the body. The trailing-edge spoilers were machined separately, pinned in place for alinement, and then silver soldered. This technique permitted easy selection of spoiler height after the models were built and was found to be satisfactory up to a launch velocity of 1000 m/sec.

The sabot used with these models was made of six parts – a rifled aluminum base that was keyed to the model to produce the rotation, four rifled nylon fingers and a copper obturation cup to prevent powder gas leakage. Since both the sabot base and fingers were rifled, the resulting high spin rate of the configuration caused rapid radial separation of the fingers from the model. The fingers were not keyed to the base since the rifling grooves provided the necessary alinement.

3.4.1.1 Gas Seals

At this point, it is worthwhile to digress a bit from model and sabot design and discuss various types of auxiliary seals and obturation cups which are often used to prevent the propelling gas from leaking around or through the sabot. These gas seals are most often used when the sabot is of the split-base type (see for example, Figure 3.13), or where it is desirable to have a loose fitting sabot in the gun initially to minimize any radial compression of the model and sabot during travel through the launch tube. (Due to erosion by the driver gas, most launch tubes develop a taper of several thousandths of a cm during normal use). These seals can take many forms and the choice is usually made on the basis of material, weight, size and condition of the gun, as well as personal experience and preference.

A very simple type of gas seal is a thin disk of neoprene rubber (3 to 6 mm thick) and about 10 percent greater in diameter than the bore of the gun. The slight cupping of the rubber forms an effective seal to prevent gas from reaching the base of the sabot. Two other types of gas seal are shown in Figure 3.15. The first is a composite seal, simply made from polyester plastic and double-sided pressure sensitive tape. This plastic seal has worked remarkably well in many types of guns up to launch velocities of 8 km/sec. The other is the so-called obturation cup, which utilizes the high-pressure propellant gas acting in the hollow cavity to provide the seal. The cup may be integral with the sabot base or may be a separate part.

3.4.2 Investment-Cast Models

The method of model fabrication discussed thus far, i.e., assembly from individually machined sub-parts, is the preferred approach as long as these parts are easily generated by machine tools and the joints are sufficiently strong to survive the acceleration loads during launch. In many cases, however, models which do not lend themselves to straightforward machining techniques are required for testing. For these models of more complicated shape, the investment-casting technique has been used. This method of casting results in precisely duplicated models which are relatively inexpensive and require little or no finishing work. Both bronze and aluminum have been used successfully for these castings. To achieve a center-of-gravity position other than that of the homogeneous model, the models could be hollowed out and, if necessary, ballasting added. Figure 3.16 shows a group of five models that were produced by the investment-casting technique and were successfully launched at velocities up to 2000 m/sec.

One example of investment cast models is that of the X-15 research airplane[3.8]. This model and its sabot are shown in Figure 3.17. The model was cast of aluminum and was launched at velocities up to 1500 m/sec using a powder-gas gun with a 57 mm bore. The driver-gas pressure was used to separate the two halves of the sabot. The halves were held apart by the shear pin and the aluminum pieces of the sabot. The resulting gap provided the volume for the driver gas reservoir. No sabot fingers were used here; alinement was achieved by a pin in the base of the model, which was gripped by the aluminum inserts in the nylon base.

The two delta-wing models shown in Figure 3.16 were also cast of aluminum. The three-wing model is shown with its sabot in Figure 3.18 (Ref.3.9) (a shadowgraph of this model in flight is presented in Figure 6.75). This model used a three-piece nylon sabot with aluminum inserts to take the concentrated load from the small base area of the fuselage and wings. The sabot is separated from the model by the powder-gas pressure which acts on the walls of a centrally-drilled hole in the sabot. Axial movement of the three segments is prevented by the short, metal shear pins. In this design an O-ring on the outside of the sabot was used as an effective seal to prevent powder gases from flowing around the sabot. The four-wing model was essentially the same in construction and used a plastic sabot which was split into four segments [3.10].

A third example of a cast aluminum model is the glider-like model shown in Figure 3.19. This model proved difficult to launch at small or moderate angles of attack because of its light weight and long trailing wings. Because of the long wings even a small disturbance by the sabot would result in large initial angles of attack. A few low-angle-of-attack flights were obtained with this model and sabot combination indicating nearly perfect sabot separation in these cases. As shown in Figure 3.19 the sabot used for this model was made of nylon,

hollowed out at the front end, and used an aluminum pedestal screwed to the base to support the model. The sabot was split in halves and was separated by aerodynamic pressure forces acting inside the hollow front end. No alinement fingers were used - the pin in the base of the model served to hold and aline the model in the sabot until the launching loads were applied.

Another example of an investment-cast model is the half-cone, lifting-body model shown in Figure 3.20 (Ref. 3.11). Bronze was used as the construction material to achieve the desired model density. This nonaxisymmetric shape trims, or flies, at a constant lifting attitude so the high weight was required to keep the flight trajectory within the walls of the facility. The model was cast with internal cavities which extended to the base to obtain the required center-of-gravity position without resorting to any internal machining or ballasting. The two pins in the base were added after the base was machined to position the model in the sabot and to provide a reference for determining the model's roll, pitch, and yaw attitudes. The sabot halves were separated from the model by the force of the driver gas trapped in the centrally-drilled hole.

3.4.3 Simple Machined Models

Other types of models which fall into the general category of being completely and easily machined are shown in the next two figures. The bimetallic model shown in Figure 3.21 was used to investigate boundary-layer transition on a highly swept wing[3.12]. This model represents a sector of the surface of a cone and thus was easily generated by machining and amenable to automatic machine polishing. The bimetallic construction was necessary to provide aerodynamic stability but resulted in an undesirable surface joint. This surface joint was a source of boundary-layer disturbance and is cited as an example of the unavoidable consequences of conflicting requirements.

Presented in Figure 3.22 are a group of models that consist of open-ended tubes. They are shown in two groups: the set shown in Figure 3.22(a) was used to study skin-friction drag[3.13] (the model on the right has a large ratio of surface area to frontal area, the model on the left is a tare model), and the other set was used to measure the drag of trailing-edge spoilers[3.6]. Both sets of models were launched successfully from rifled guns using solid metal pre-rifled bases as shown in Figure 3.22(b). In addition, the surfaces of the skin friction models were separated and protected from the lands of the rifling by a simple wrap of photographic film, held in place with cellophane tape during loading into the gun. A number of pre-rifled nylon supporting pieces were used with the solid metal base to launch the spoiler models. The centrifugal forces developed by the rifling quickly separated the sabot pieces from the model upon emergence from the gun.

The use of saboted models for ballistic testing is not limited to the sizes indicated thus far in this chapter. Large guns, such as the 127 mm, 178 mm, and 406 mm diameter guns used in high altitude research (HARP)[3.14,3.15] have launched very large saboted and instrumented models into the upper atmosphere. For example a model used in the 406 mm gun weighed about 84 kilograms and was launched at a velocity of approximately 2000 m/sec. The sabot base was aluminum with a steel insert and the supporting fingers were plywood. The capability of the 406 mm gun is impressive; models have been projected to a height of approximately 143 kilometers. Although these tests lie somewhat outside the realm of typical ballistic-range tests, they represent the largest models for use in ballistic research as well as the longest "instrumented" range.

3.5 MODELS AND SABOTS FOR HIGH-SPEED TESTS

Although the design approach outlined earlier is an almost essential companion to designing successful high speed models and sabots, it does not assure *a priori* that success will be obtained when the model is launched. This may be because the dynamic or transient loads imposed on the configuration during launch are not well enough understood to be evaluated accurately, or it may be because a failure mode has been overlooked entirely. Therefore, it can be said that the design of models and sabots for use at high speeds is strongly guided by design techniques which have proven successful in the past – i.e., the design is highly empirical.

It is therefore very pertinent to review designs which have been successful. In doing so we will examine some relatively complex and fragile models which have worked well at speeds up to 8 km/sec, as well as some simple configurations which have been launched at speeds up to 11.3 km/sec.

3.5.1 Design and Construction of Typical Models

The first configuration which we will consider is shown in Figure 3.23. Tests of this configuration were conducted in a pressurized ballistic range of the US Naval Ordnance Laboratory[3.16,3.17]. The models were homogeneous steel bodies, hollowed out to obtain aerodynamic stability. This type of construction results in the lightest possible model weight for a given material and represents the simplest approach to model design. The plastic sabot used to launch the models is also shown in Figure 3.23. Plastics are generally used as sabot material because they are sufficiently strong and lightweight, accommodate the small irregularities of the launch tube well, cause no appreciable wear of the launch tube, and because of their lightweight, inflict less damage to the test facility after emerging from the gun. Polycarbonate plastic (Lexan) is used widely because it has both a higher impact strength and a high modulus of elasticity than most other plastics. This type of sabot has proven very successful in launching models at high speeds and so is common in ballistic-range work. It features four polycarbonate fingers which fit around the model and are separated from it by aerodynamic forces acting on the beveled front faces. Polycarbonate pins are used to prevent longitudinal shifting of the fingers in the gun. The thin titanium plate distributes the model weight into the base of the sabot fingers. The separate polycarbonate base piece is also commonly used to more evenly distribute the pressure loads to the base

of the fingers and also as a gas seal. In this particular sabot, linen-phenolic inserts were used to aline the model in the sabot fingers (rather than thickening the fingers to mate to the model) which results in a lower total weight and a lower ballistic coefficient, m/C_DS, for each of the fingers, both of which provide for better separation of the fingers from the model. In later sections of this chapter it will be seen that the same basic components as these just described were used in other sabot designs; therefore, in these cases, it will be necessary only to present a photograph of each sabot and to point out important modifications.

A different design approach to the configuration just described is illustrated in Figure 3.24 (Ref.3.18, 3.19). The aftersection of each of these models was solid and was machined from 7075-T6 aluminum; the front sections of the models with and without afterbody were machined from phosphor bronze and titanium, respectively, to obtain the same center-of-gravity location (0.48d from the nose) as the model discussed previously. As can be seen, the nose ballast materials were attached to the aluminum aftersections by means of a screw of the ballast material. The small screw on the base of the flat-based model was used to secure the model to the sabot and the point on the base of the screw served as a measurement reference in the shadowgraph pictures. The sabots for these models differed from the one shown in Figure 3.23 in that they were made in two pieces; a hole drilled in the center allowed gases inside the sabot to separate the two halves from the model upon emergence from the gun.

Figures 3.25, 3.26 and 3.27 show sketches of three other bimetallic models. The noses of all three were machined from a sintered tungsten alloy and threaded into an aftersection machined from 7075-T6 aluminum. The configuration shown in Figure 3.25 (Ref.3.20) was launched using a sabot machined from ethyl cellulose plastic, split in two pieces, and having a hemispherical aluminum load-bearing insert under the model. The model is shown in one half of the sabot in Figure 3.25. The ballasted-sphere model[3.21] shown in Figure 3.26 was launched from a caliber 50 deformable piston light-gas gun similar to the one described in Reference 3.22 using the sabot shown. The noses of the first two models launched with this type of sabot broke off for a rather obscure reason. Each of these first two sabots had an oversized hole to accommodate the stud at the base of the model, which in this case was necessary to define the model's angle of attack in the shadowgraphs. Although the sabot held the model in place by gripping it above the maximum diameter, the model could pitch a few degrees in the sabot before the stud made contact with the wall of the hole. This skewed attitude led to shearing of the screw that held the nose to the aftersection. In succeeding tests the diameter of the hole in the sabot was made the same as that of the stud and resulted in successful launches being obtained. Tests of this model at 4 km/sec through air at one atmosphere were precluded because the tungsten-alloy nose material came apart or spalled under the high-heating rates experienced during flight. A shadowgraph from one of these flights showing this spallation is presented in Figure 8.37.

The configuration shown in Figure 3.27 (Ref.3.23) was launched at velocities of 3 km/sec and 4.6 km/sec into still air at a static pressure of 0.4 atmosphere. The models launched at 4.6 km/sec survived the launch but the tungsten-alloy nose material, as in the preceding example, spalled under the high-heating rates experienced in flight. A successful method of heat protection for the model was therefore devised and will be described in Section 3.5.2 of this chapter. These models were initially launched by means of the sabot shown in Figure 3.27. However, the models were so statically stable that they had to be canted in the sabot by as much as 15° to obtain data at angles of attack above about 5°. Unlike the case of the ballasted sphere, the noses of these models did not break off as a result of the model's skewed attitude in the gun.

A different design approach was necessary for the configuration shown in Figure 3.28 (Ref.3.24) to keep the nose screw of the model from repeatedly breaking off at the joint during launch. Note the very small scale of these models - 3 mm body diameter. A separate steel machine screw, which is stronger than the tungsten alloy, was used to fasten the tungsten-alloy nose to the 7075-T6 aluminum aftersection. One end of this steel screw extended through the nose and was machined to form the center of the front face; the other end was hemispherical and bottomed, with essentially zero clearance, into the hole machined in the aluminum section. This trimetallic design permitted these small models to be successfully launched at speeds up to 6.5 km/sec. While the resultant velocity (i.e., model velocity plus countercurrent flow velocity) was high (8.2 km/sec), the free-stream density for these tests was low (ρ_∞ = 0.03 atmosphere), and no spalling of the nose material was evident in the shadowgraph pictures. A photograph of the four-piece sabot (three polycarbonate fingers and a partly hollow polyethylene base seal) used to launch these models is presented in Figures 3.28.

A trimetallic model design was also used successfully for the configuration shown in Figure 3.29 (Ref.3.25). In this case also, a steel machine screw was used to attach a rather large nose piece machined from a tantalum alloy containing 90 percent tantalum and 10 percent tungsten (Ta - 10w), to an aftersection machined from 7075-T6 aluminum. This combination of materials, in addition to the hollowing of the base shown, gave the desired center-of-gravity position. Sintered tungsten alloy was originally used as the nose material but it blunted significantly during the flight and was so replaced with the tantalum alloy which survived the flight with little blunting. These models were launched in the nose-forward attitude using the sabot shown at the left in Figure 3.29. To help prevent possible separation of the nose from the aftersection during the launch, the two polycarbonate fingers of the sabot were designed to completely encapsulate the model. By this technique, the tip is strengthened against convergence of stress waves. It is interesting to note that this technique of encapsulating a model within a sabot was used in early ballistic-range work to prevent "curling" or bending of the tip of a slender cone when launched at relatively low speeds from powder gas guns.

To test their stability in a backward orientation, these models were launched in the base-forward attitude by means of the sabot shown at the right in Figure 3.29. To provide support for the model in this attitude, aluminum inserts contoured to match the model geometry were screwed to the inside of the polycarbonate fingers. This

rigid support prevented the model from being driven through the base of the sabot by the launch acceleration and permitted successful launching of the model at a velocity of 4 km/sec with no damage to the sharp tip.

Figure 3.30 shows a sketch of an Apollo-Type command module model, where a radial movement of the center of gravity of approximately 0.045 d was required to produce a trim angle of attack of 30 degrees (Ref.3.26). This radial offset of the center of gravity was achieved by use of a cylinder of sintered tungsten alloy and a cylinder of magnesium pressed into a block of 4340 steel before machining the assembly to the desired geometry with a smooth external surface. This model was made heavy to limit the flightpath curvature due to lift. The polycarbonate sabot used to launch the models at the natural trim attitude was split in two pieces along its plane of symmetry as shown in Figure 3.30. Two small peened-over sections of the sabot lip (180^{o} apart) held the model in the sabot before launch.

One of the most complex and fragile models ever tested at speeds above 6 km/sec in a ballistic range is illustrated in Figure 3.31 (Ref.3.27). This small-scale model of an Apollo command capsule used a passive telemetry system (see Chapter 12) to measure afterbody heating during flight. Each model was constructed from no less than eight parts, which were glued together with epoxy glue. All electrical connections in the model were soft-soldered. A photograph showing the individual components along with an assembled model is presented in Figure 3.31. Several of these models were launched successfully at velocities up to 6.1 km/sec and the desired in-flight data were obtained. A sketch of the sabot used to launch the models is also shown in Figure 3.31.

3.5.2 Methods of Heat Protection

For speed above about 4 km/sec and for lower speeds when the free-stream density is high, a primary concern, particularly for pointed bodies such as cones, may be heat protection during flight. The need for heat protection is evidenced by melting or ablation leading to unacceptable rounding of sharp-tipped models, chemical burning of models in flight (Chapter 8), or spalling of model surfaces. There are three ways in which the model designer can solve these problems. One is to use metals that can be subjected to very high heating rates without melting. Whether or not a particular metal will melt during flight at particular test conditions can be ascertained by use of the following equation derived by Carslaw and Jaeger in Reference 3.28 for the time to reach melting temperature

$$t_m = \left[\frac{(T_m - T_0)K}{2\dot{q}}\right]^2 \frac{\pi}{k}, \tag{3.12}$$

where

t_m time to reach melting temperature at a particular point on the cone surface

T_m melting temperature

T_0 initial temperature

K thermal conductivity

k thermal diffusivity

and $\dot{q}$ is the stagnation point heating rate, which depends on test conditions and model geometry and is given by the equation $\dot{q} = C_H \frac{1}{2}\rho_\infty V_\infty^3 S$, where C_H is the heat-transfer coefficient, ρ_∞ and V_∞ are the free-stream density and velocity, respectively, and S is the model base area. The heating rate, $\dot{q}$, along the sides of the cone varies as $1/\sqrt{x}$ (x is axial distance along the cone). It is seen from Equation (3.12) that the time required to reach melting temperature is greatest for materials that have a high-melting temperature, high thermal conductivity, and low thermal diffusivity. Since the thermal diffusivity, k, is equal to the thermal conductivity, K, divided by the product of the material density, ρ_m, and specific heat, c, it is helpful to write Equation (3.12) in the form

$$t_m = \frac{(T_m - T_0)^2 K \rho_m c \pi}{4\dot{q}^2}. \tag{3.13}$$

It is seen from Equation (3.13) that a material having a high value of the product of $\Delta T^2 K \rho_m c$ will have the longest flight time before starting to melt. Since the time to melt varies as the square of the melting temperature, metals with very high melting temperatures such as tungsten (3680^{o}K), tantalum (3320^{o}K), and molybdenum (2900^{o}K) are the best metals to use for this purpose. It is important to recall here that these dense metals are also good ballast materials.

The second approach to the heat protection problem is to use plastics which undergo ablation during flight. The ablation gases coming off the model surface inhibit convective heating and minimize the mass loss. Plastics such as polytetrafluoroethylene (Teflon), Acetal (Delrin), Polycarbonate (Lexan), Polyethylene, Nylon, and Phenolic Nylon, have performed very satisfactorily in this respect. The amount of nose blunting and surface recession they experience is often acceptable to speeds of 10 km/sec. It is important to state here that all aerodynamic measurements such as static and dynamic stability, drag, lift, etc., made from flights where ablation of the surface is taking place at a high rate, must be considered as aerodynamic characteristics of "ablating" models. The aerodynamic characteristics of slender bodies are known to be strongly influenced by ablation. Nonablating models of the same geometry may have significantly different aerodyanmic characteristics (see, for

example, References 3.29 and 3.30). A study of the feasibility of obtaining aerodynamic data on ablating slender cones in a ballistic range is presented in References 3.31 and 3.32.

The third approach to the heat-protection problem is to use plastics but still not forfeit the advantages of metals. Thin ablative heat shields have been applied over metal bodies to combine heat protection through surface ablation and the high physical strength afforded only by metals. However, bonding these thin plastic coatings to metal models is not always simple and requires development of techniques to obtain good strength without weakening the metal structure. In the following paragraphs, examples are given of particular materials and model and sabot designs used successfully in high-speed tests where high heating rate was one of the problems to be overcome.

A solution of the first type, that is, metals with high melting temperatures, was used for the models shown in Figures 3.32 (Refs.3.31,3.32), and 3.33 (Ref.3.33). For the 10^{o} half-angle cone (Fig.3.32) a tantalum nose was threaded into the aluminum aftersection. These slender cones have been successfully launched at speeds up to about 6 km/sec into still air at a range pressure of 0.04 atmosphere and experienced little blunting of the nose during flight. The sabots used to launch these models are also shown in the figure.

The 6^{o} 20′ half-angle cone shown in Figure 3.33 used a pure tungsten nose silver-soldered to a hollow, titanium alloy aftersection to alleviate tip blunting. Since these two materials could not be threaded together because it is nearly impossible to machine threads on pure tungsten, a silver soldering technique was used to join the two materials. The soldering method used was unique in that the silver-solder adheres to the pure tungsten stud but forms a mechanical junction with the titanium alloy aftersection by means of two rings machined into the walls of the hole which accommodates the stud. The sabots used to launch these models (Fig.3.33) are seen to be nearly identical to those presented in Figure 3.23. These four sabot fingers were made of linen-phenolic to provide strength and minimize weight and used a separate two piece cylindrical center section to accommodate the model. Use of the center section enabled straight-forward machining of the model cavity from one end.

A homogeneous plastic 30^{o} cone, an example of the second heat protection method, the ablating model, is shown in Figure 3.34; this model was successfully launched at high speed and survived the high-heating conditions of the flight with no significant nose blunting or surface recession[3,34]. These models were made of solid polytetrafluorethylene (Teflon), a relatively weak material (Table 3.1)*. Successful high-speed launching of these solid Teflon cones was not attained until the completely encapsulating sabot shown in Figure 3.34 was used; all other attempts failed. Note in Figure 3.34 that it was necessary to make the polyethylene base piece (also, gas seal component of this sabot) very thin (1.2 mm) so that it would decelerate rapidly relative to the model.

Acetal plastic (Delrin) has also been used successfully at high-speed, and survived the heating during flight with little nose blunting and surface recession in the slender cone configuration shown in Figure 3.35 (Refs. 3.31,3.32). The sabot base piece used to launch these models at velocities up to 6 km/sec was polyethylene. It is interesting to note that gun performance limited the velocity of these tests rather than any structural limitation of the model-sabot combination.

The third and sometimes most desirable method of heat protection in high speed flight, that of using a relatively thin plastic coating over a metal model, is illustrated by the two configurations, in Figures 3.36 (Ref. 3.35) and 3.37 (Ref.3.23). The first configuration, a 30^{o} half-angle cone, used a polyethylene outer sleeve which was injection molded over an aluminum (7075-T6) core. The models were then re-machined and trimmed to give the desired dimensions and were launched using the sabots shown in Figure 3.36. The polyethylene sleeve survived launching, provided heat protection to the model, and suffered little shape change during the course of the flight.

A much thinner plastic coating was found to provide a successful heat shield for bimetallic models of the configuration shown in Figure 3.37. The coating consisted of vinylidene fluoride polymer sprayed onto the model surface to a thickness of about 0.04 cm. The models were re-machined and trimmed to give a final coat thickness of about 0.02 cm. As can be seen from a comparison of Figure 3.37 with Figure 3.27, these configurations are the same but use different materials for the aftersections. The plastic-coated models required titanium alloy since the heat-curing cycle of the plastic was found to anneal the aluminum so that it deformed severely during the launch. The strength of the titanium alloy was not affected by the curing. Since titanium is heavier than aluminum, the size of the tungsten alloy front section was adjusted to achieve the same center-of-gravity location as for the earlier models. The coated models survived the heating with no significant nose blunting or surface recession. This is demonstrated by the shadowgraphs of one of these models at the first and last observation stations of the Ames Prototype Hypervelocity Free-Flight Facility shown in Figure 3.37.

3.5.3 Models For Maximum Speed Tests

Ballistic range tests such as those conducted to study radiation emitted by the shock layer ahead of a model (and also by the wake flow), to study impact phenomena, and also to study ablation and/or spalling of bodies simulating the behavior of meteorites, usually require the maximum model velocity attainable using the best guns available. Launching models from presently available light-gas guns at speeds above about 7.5 km/sec produces accelerations in excess of about 2×10^{6} gravities; therefore only very small simple models can be used successfully. Fortunately, useful data can be obtained using these models. In this section, some representative examples of models of this type will be discussed.

* A homogeneous cone having a half-angle greater than 19.5^{o} is aerodynamically stable – no ballasting is necessary.

An important category of models here is the full caliber plastic model launched without a sabot. Most of these models, especially those used to make radiation measurements, consist of a short cylinder of plastic with the front face contoured to the particular shape of interest, such as flat, spherical or conical. The cylinder length for these models is usually about one-third caliber, or greater, for stability in the launch tube.

A sketch representing two full-bore plastic models, one of the type that achieved the highest velocity ever attained by an undamaged model in a light gas gun (11.3 km/sec), and also of the type frequently used in gas cap radiation studies, is presented in Figure 3.38. The full-bore right circular cylinders are machined from high-density polyethylene, polycarbonate, or other plastics. The model which achieved the highest velocity was successfully launched from a .22 caliber gun into a quiescent nitrogen atmosphere at a static pressure of about 1 torr (Ref.3.36).

At times, however, meteorite simulation studies and impact studies require firing very small (sub-caliber) models. In these cases a sabot is necessary. Figure 3.39 shows photographs of one such "model" and sabot combination which was launched successfully at speeds of about 8 km/sec from a caliber 30 deformable-piston light-gas gun at range pressures of about 0.03 atmosphere. The models were spherical particles of crystalline aluminum oxide (Al_2O_3) of from 400 to 700 microns diameter. Despite the high g loading, the very small weight of the particles kept stress levels below the strength of the materials. It was concluded in Reference 3.37 that mechanical breakup or disintegration of these aluminum oxide microspheres occurred during flight at these test conditions due to the thermal stress induced in the sphere by the temperature gradient in the particle. The thermal stress induced in the sphere was calculated using the following equation given by Timoshenko in Reference 3.38:

$$\sigma_T = 0.771 \frac{\alpha E}{2(1-\nu)} (T_m - T_0) , \qquad (3.14)$$

where

T_m melting temperature

T_0 initial temperature

α temperature coefficient of expansion

E elasticity modulus

ν Poisson's ratio,

and was found to be about an order of magnitude greater than the maximum tensile strength of the aluminum oxide, which is approximately 40,000 lb/in^2.

The serrated sabot used in these tests offers very high resistance to differential shearing of the four pieces. A further description of this interesting sabot type and its use are presented in Reference 3.39. A photograph of a cone model with a four-piece serrated sabot taken from this reference is presented in Figure 3.40.

Other examples of small saboted metal or glass spheres and a saboted thin polyethylene disc which have been successfully launched at speeds of about 9 km/sec are presented in Figures 3.41 to 3.44; pertinent information concerning the models and sabots are given in the table in each of the figures. An adhesive with little impact strength was used to hold the 600 micron diameter steel sphere in a small cavity on the front face of the sabot shown in Figure 3.41 before launch. The sabots shown in Figures 3.41 and 3.42 were separated from the models by aerodynamic forces acting on the front face. The sabots shown in Figures 3.43 and 3.44 were fired from a rifled launch tube and upon emergence from the gun, the centrifugal forces split and separated the sabot pieces from the models.

3.6 PHYSICAL MEASUREMENTS OF MODELS

A very important aspect of ballistic range testing of models is the determination of their physical characteristics prior to the test. The physical properties include dimensions and angles, mass, and moments of inertia. Accurate measurement of these properties is essential, since errors incurred here can lead to significant errors in the final results. Some of these properties are easy to measure accurately - e.g., diameter with a micrometer; others are very difficult to characterize, e.g., surface roughness. A discussion of some of the techniques used to make these measurements will be given in the following paragraphs.

3.6.1 Determination of Model Mass

The mass of a model is easily and accurately determined by use of a good analytical balance of either the equal-arm type (Fig.3.45(a)) or the substitution type (Fig.3.45(b)). For the equal-arm type, the model is placed on one of the pans and known weights added on the other pan until equilibrium is reached. The sum of the known weights is then equal to the model mass. For the substitution type, the model is placed in a pan, and known weights, which are built into the balance, are removed from the same end of the balance beam until equilibrium is achieved. Both types of analytical balances are easily accurate to 0.1 milligram, which, for models of the sizes described earlier, provides accuracy to a small fraction of one percent.

3.6.2 Determination of Model Center of Gravity

The center of gravity of a model can be determined by use of a modified analytical balance of the equal-arm type (see Figure 3.46). As shown in this figure, a plate which holds the model is attached to one end of the balance beam at an accurately known distance from the fulcrum. (The pan on this end of the beam is not needed and is therefore removed.) Known weights are placed in the pan at the opposite end of the balance beam until equilibrium is achieved. The distance between the model's center of gravity and the base of the model (front face of the plate) is then computed using the following equation:

$$X_{CG} = X_R \frac{m - m_{tare}}{M} - X_L \ , \tag{3.15}$$

where (see sketch in Figure 3.46)

M model mass

m sum of known weights necessary to achieve balance equilibrium

m_{tare} sum of known weights necessary to achieve balance equilibrium with no model

X_R distance from fulcrum to support point of pan

X_L distance from fulcrum to base of model.

The distances X_R and X_L are accurately determined by prior calibration of the balance using models with known centers of gravity such as accurately machined right circular cylinders. By this method, the centers of gravity of models can be determined to within 0.025 mm. This precision is usually quite adequate, however, the error in this measurement should always be compared to the model's static margin to assess its effect on the final results.

3.6.3 Determination of Model Moments of Inertia

To determine the aerodynamic stability characteristics, the moments of inertia of the model must be known. A simple method for measuring the moment of inertia of a body is by the use of a torsion pendulum. The period of oscillation of a torsion pendulum is

$$T = 2\pi \sqrt{\left(\frac{I + I_0}{C_0}\right)} \ , \tag{3.16}$$

where

I_0 tare moment of inertia (should be small relative to model)

C_0 constant, dependent on wire diameter and length

I moment of inertia of model.

A sketch of a typical torsion pendulum setup is shown in Figure 3.47. By placing cylinders of known moments of inertia in the holder, the value of C_0 and I_0 can be determined by measuring the periods of oscillation. Then, by measuring the period with the model in the holder, the moment of inertia of the model can be computed. With sensibly chosen torsion wires and calibration cylinders, values of the model moment of inertia can be determined accurate to a fraction of one percent*.

A photograph of an apparatus used for moment-of-inertia measurements is presented in Figure 3.48. The wire and holder with a model attached are seen to the right in the figure. The model holder has a polished face which reflects a light beam from a fixed source to a photocell. The light beam serves to trigger the electronic counter. To eliminate the problem of centering the oscillation, the counter is triggered on alternate pulses emitted by the photocell. This method gives the time for one complete cycle.

3.6.4 Surface Finish Measurements

In ballistic-range tests intended to study boundary-layer transition on a model (see for example, Figure 3.21), the surface finish of the model must be controlled very precisely. This requires very accurate measurements of the amount and type of surface roughness present or produced on the model by machining, polishing, etc. For accurate measurements of surface roughness it is almost imperative that the techniques used do not mark, alter, or destroy the surface in any way. The use of instruments which contact the surface for example and trace the profile of roughness in the manner of a phonograph needle has been shown to be both inaccurate and damaging to the surface. Photomicrographs of the paths traced along the surface show that, even with a very light bearing force (on the order of a fraction of a gram), the sensing contact produces a furrow in the surface. Thus, it plows through the small grain roughness which is of interest in boundary-layer-transition work and in addition, leaves a scratch on the surface which has a width of the order of the tip diameter of the sensor and a depth which is proportional to both the bearing force of the sensor and the hardness of the model material.

---

* Length and diameter of the wire should be such that the period of oscillation is of the order of 1 to 2 seconds.

Two methods of surface finish measurements which meet this requirement and give accurate results are the multiple-beam interferometer and the wire shadow method. Both of these methods are described in detail in Reference 3.40. The first method uses green light with a wavelength of 5461 Å to produce a fringe pattern whose contour lines represent an elevation height of 274×10^{-6} mm. The second method, the wire shadow technique, utilizes a line shadow cast obliquely on the surface in question. Irregularities in the surface will produce an irregular shadow whose deviations can be measured with a microscope.

3.7 SABOT SEPARATION DEVICES AND SABOT TRAPS

As discussed in earlier sections of this chapter, the four basic methods used by the designer to achieve adequate separation between model and sabot before the model reaches the test area are:

(a) Design sabot parts which will produce large lift and/or drag forces and thus cause these pieces to fly away from the line of boresight and/or decelerate quickly behind the model. Success of this technique depends primarily on the ambient pressure outside the muzzle of the gun.

(b) Use the pressure force of the propellent gas acting in cavities at interfaces of the sabot base pieces and also sabot fingers to separate these pieces radially away from the model.

(c) Provide mechanical devices to decelerate the sabot and deflect it to one side. These devices will have their greatest use at very low ambient pressures.

(d) Use a sectioned sabot in a rifled barrel. The high tangential velocity of each piece carries it away from boresight and is independent of ambient pressure.

In some sabot designs employing the first method (i.e., aerodynamic forces), the sabot fingers separate radially from the model initially but then remain in close formation around the model during the entire flight. These segments can usually be stopped short of the test section by allowing them to impact into a steel plate which has a hole in the center large enough to allow only the model. A shallow-angle steel cone with a similar hole is sometimes added to the flat plate to make the initial impact oblique (and therefore less violent), and to force the sabot pieces radially outward. Of course this sabot trap will only be successful if there is a sufficiently high air density to provide an initial radial separation of the fingers.

For tests at low pressures, where the aerodynamic forces might not be adequate, a small tank with a higher static pressure can be used between the test section and gun[3.41]. A tank of this sort can be, in its simplest form, merely a length of tubing such as is shown in Figure 3.49. The entry and exit to this tank are sealed using thin plastic diaphragms. The entry diaphragm which is usually at the muzzle of the gun is broken either by the model and/or sabot or by the compressed air ahead of it. In the tank the high pressure air separates the sabot from the model, and the sabot segments are caught by the sabot trap as before. The model flies into the test section through the second diaphragm. In some tests, models cannot be permitted to fly through even these thin diaphragms because of the possibility of damage to sharp tips, leading edges or surface finish. In these cases the plastic diaphragms can be ruptured on signal with punches or exploding wires, or they might be replaced by quick-opening valves.

Extra care must be taken with this air-tank procedure to insure that the model receives negligible angular disturbance during the sabot separation process. If the model is pitched and enters the low pressure test section with excessive pitching rate, there could be insufficient restoring moment at this lower pressure to prevent the model from tumbling. If this disturbance is unavoidable but fairly repeatable it might be possible to adjust the muzzle position and air tank pressure so the model enters the low-pressure section at nearly maximum pitch amplitude (and low pitching rate), thus limiting the final amplitude.

In counter-flow facilities, as mentioned in Chapter 5, the shock-tube-wind-tunnel receiver tank (dump tank) has been used as the high-pressure sabot-separation tank. With the counter-flow air stream, the exit diaphragm (between the test section and the dump tank) is removed by the tunnel flow. Also, in this type of facility, the static pressure of the still air in the dump tank can be adjusted so that the dynamic pressure experienced by the model flying in this still air is equal to the dynamic pressure experienced during flight through the counter-flow air stream, hence, the model experiences no large changes in restoring moment in moving from one regime to the other.

For the case of a solid sabot base, it is often necessary to mechanically remove the piece from the flightpath using some type of sabot decelerator together with a deflector. The most successful devices for diverting these sabots are the contracting tube with a deflecting section or separate ramp[3.41,3.42]. The decelerator is a muzzle extension of contracting bore diameter with gas-release ports, Figure 3.50. The model and sabot enter this contracting section which then squeezes and decelerates the sabot base during the entire travel through the barrel extension. The driving gases are diverted out the ports in the wall. The model, which must be subcaliber, leaves the sabot and continues at launch speed. The sabot then strikes a deflecting ramp, or is deflected by the barrel (see Figure 3.50) and is diverted off the flight line of the model and into a retaining plate. The ramp and deflecting barrel are positioned so that the model passes undisturbed into the range. Another version of this simple sabot decelerator is merely a plate, with a subcaliber hole, attached to the muzzle of the gun which decelerates the sabot by shearing off a thickness of the sabot's outer wall material. This type of decelerator was used to separate the model and sabot shown in Figure 3.12.

As noted earlier, separation of a finger type or split sabot from the model can be achieved using a rifled launch tube in tests where model spin is either desirable or not detrimental. In impact studies, where positive separation is demanded and only the model must strike the target, rifled barrels have been used at velocities up to 9 km/sec.

3.8 PROOF TESTING

With a newly designed model and sabot, it is usually necessary to conduct proof tests. When these tests are made, frequently the initial design is not completely successful; i.e., it fails to put the model into flight undeformed and intact, or it imparts excessive disturbance to the model at sabot separation, or the sabot does not separate widely enough from the model. Quite often, when a new design is tried only fragments of the model and/or sabot will pass through the instrumented stations of the test facility. In these cases, it is very difficult to determine the exact cause of model and/or sabot failure.

In such cases, additional instrumentation is often required, usually to obtain more information on events occurring near the gun muzzle. For example, if the condition of the model and sabot can be determined just as they emerge from the gun, it may be possible to conclude whether a structural failure occurred in the model or in the sabot, and whether the failure is due to a misalinement in the launch tube or whether the entire problem is in the model-sabot separation sequence. To accomplish this, X-ray photographs have been taken at the muzzle to determine the structural integrity and relative orientation of the parts.

The use of X-ray photography is advantageous, since such pictures can be taken in the presence of very bright muzzle flashes, which would completely blacken ordinary visible light photographs. An example of an X-ray photograph is presented in Figure 3.51. Also, a series of X-ray photographs taken at various distances from the gun muzzle in separate launchings of identical model-sabot combinations is presented in Figure 6.27. However, pictures like these are not easily obtained, and usually require a significant investment of time and effort in setting up the equipment, devising and testing suitable triggers, etc.

Pictures near the muzzle have also been obtained with high speed motion pictures cameras, looking toward the muzzle with telescopic lenses from a safe distance. The muzzle flash can provide back lighting for such pictures, and the sabot separation sequence can be recorded in silhouette. However, the number of frames is limited, even with cameras operating at 5000 to 7000 frames per second and frequently the model is not seen until it emerges from and outruns the muzzle blast. The critical events may by this time already be past.

Yaw cards (Chapter 6) are also useful for diagnosing separation difficulties. The relative positions and attitudes of model, sabot fingers, sabot base, etc., can be well identified, and used as a basis for constructing motion histories of the parts. These can give considerable insight as to whether the separation is taking place as planned. Model failures can also be diagnosed in this way – e.g., a bent or broken tip is conspicuously evident, as are other missing or separated sections of models. A problem with yaw cards is that they are normally torn into small pieces by the muzzle blast, and these pieces must be painstakingly gathered and fitted together. At very high launch velocities, the cards are essentially demolished, and the parts may not be recoverable and may even burn. Hence, this technique has very definite limitations.

When the development process is successfully completed, which may take several iterations in the design, and the model is launched in good condition, at the proper attitude and with small disturbance, the end objective of the design work described in this chapter has been achieved. Then it is possible to proceed, using these models to conduct the various types of tests which will be discussed in the following chapters.

REFERENCES

3.1 Watson, J.D.; Godfrey, C.S. — *An Investigation of Projectile Integrity Using Computer Techniques.* PITR-67-10, Physics International Co., 1967.

3.2 DeRose, Charles E.; Boissevain, Alfred G. — *An Exploratory Investigation in a Ballistic Range of the Stability Derivatives of a Simple Airplane Configuration at Low Supersonic Speeds.* NASA TN D-139, Dec. 1959.

3.3 Warren, H.R.; Templin, R.J.; Cheers, B. — *Aeroballistic Range Measurements of the Performance and Stability of Supersonic Aircraft.* Presented at 26th annual meeting of IAS, Jan. 27-30, 1958.

3.4 DeRose, Charles E. — *Ballistic-Range Tests of a Drag-Ring Configuration at Mach Numbers Around 2.* NASA TN D-4291, Dec. 1967.

3.5 Kruse, Robert L.; Short, Barbara J. — *Comparison of Free Flight and Wind Tunnel Data for Apollo Launch Escape Vehicle at Mach Numbers 0.7 and 1.2.* NASA TM X-1196, Jan. 1966.

3.6 Canning, Thomas N.; DeRose, Charles E. — *Drag and Rolling-Moment Effectiveness of Trailing-Edge Spoilers at Mach Numbers 2.2 and 5.0.* NACA RM A55F15, Oct. 1955.

3.7 Boissevain, Alfred G. — *Experimental Investigation of the Damping in Roll of Cruciform Triangular Wing-Body Combinations at Mach Numbers from 1.5 to 6.0.* NACA RM A54B15a, April 7, 1954.

3.8 Boissevain, Alfred G.; Intrieri, Peter F. — *Determination of Stability Derivatives from Ballistic Range Tests of Rolling Aircraft Models.* NASA TM X-399, Jan. 1961.

3.9 Seiff, Alvin; Wilkins, Max E. — *Experimental Investigation of a Hypersonic Glider Configuration at a Mach Number of 6 and at Full Scale Reynolds Numbers.* NASA TN D-341, Jan. 1961.

3.10 Sammonds, Robert I. — *The Shock Wave Patterns on a Cranked Wing Configuration.* NASA TN D-346, Nov. 1960.

3.11 DeRose, Charles E. — *The Aerodynamic Characteristics of a Blunt Half-Cone Entry Configuration Obtained from Ballistic Range Tests at Mach Numbers near 3.* NASA TM X-578, Oct. 1961.

3.12 Chapman, Gary T. — *Transition of the Laminar Boundary Layer on a Delta Wing with 74° Sweep in Free Flight at Mach Numbers from 2.8 to 5.3.* NASA TN D-1066, Aug. 1961.

3.13 Sommer, Simon C.; Short, Barbara J. — *Free-Flight Measurements of Turbulent Boundary Layer Skin Friction in the Presence of Severe Aerodynamic Heating at Mach Numbers from 2.8 to 7.0.* NACA TN 3391, March 1955.

3.14 Murphy, Charles A.; Bull, Gerald V.; Edwards, Howard D. — *Upper Atmosphere Winds Measured by Gun-Launched Projectiles.* BRL Memorandum Report No. 1747, May 1966.

3.15 Marks, S.T.; Pilcher, J.O. II; Brandon, F.J. — *The Development of a High Acceleration Testing Technique for the Electronic Instrumentation of HARP Projectile Systems.* BRL Memorandum Report No. 1738, March 1966.

3.16 Jaffe, Peter — *Hypersonic Ballistic Range Results of Two Planetary Entry Configurations in Air and Carbon Dioxide/Nitrogen Mixtures.* TR No. 32-543, JPL, 1964.

3.17 Crogan, Leonard E. — *Summary Report on R-71 Program.* NASA CR 55543, NOL, Jan. 1964.

3.18 Intrieri, Peter F. — *Free-Flight Measurements of the Static and Dynamic Stability and Drag of a 10° Blunted Cone at Mach Numbers 3.5 and 8.5.* NASA TN D-1299, 1962.

3.19 Compton, Dale L. — *Free-Flight Measurements of Drag and Static Stability for a Blunt-Nosed 10° Half Angle Cone at Mach Number 15.* NASA TM X-507, 1961.

3.20 Kirk, Donn B.; Miller, Robert J. — *Free-Flight Tests of Fifth-Stage Scout Entry Vehicle at Mach Numbers of 5 and 17.* NASA TN D-1425, 1962.

3.21 Short, Barbara J. — *Dynamic Flight Behavior of a Ballasted Sphere at Mach Number from 0.4 to 14.5.* NASA TN D-4198, 1967.

3.22 Curtis, John S. — *An Accelerated Reservoir Light-Gas Gun.* NASA TN D-1144, 1962.

3.23 Intrieri, Peter F. — *Study of the Stability and Drag at Mach Numbers from 4.5 to 13.5 of a Conical Venus-Entry Body.* NASA TN D-2827, 1965.

3.24 Kirk, Donn B.
Chapman, Gary T.
Free-Flight Tests of a Blunt-Nosed Flare-Stabilized Body at Speeds to 8.2 km/sec. *Journal of Spacecraft and Rockets.* Vol.3, No.3, March 1966, pp.374-377.

3.25 Malcolm, Gerald N.
Stability and Drag Characteristics at Mach Numbers of 10 and 26 of a Proposed Slender Atmospheric Probe. NASA TN D-3917, 1967.

3.26 DeRose, Charles E.
Trim Attitude, Lift and Drag of the Apollo Command Module with Offset Center-of-Gravity Positions at Mach Numbers to 29. NASA TN D-5276, June 1969.

3.27 Yee, Layton
Free-Flight Measurements of Heat Transferred to the Apollo Afterbody With and Without Heat Shield Ablation. NASA TM X-1096, 1965.

3.28 Carslaw, H.S.
Jaeger, J.C.
Conduction of Heat in Solids. Clarendon Press, Oxford, 1947, First ed.

3.29 Syvertson, C.A.
McDevitt, J.B.
Effects of Mass Addition on the Stability of Slender Cones at Hypersonic Speeds. AIAA Journal, Vol.1, No.4, 1963, pp.939-940.

3.30 Chrusciel, G.T.
Chang, S.S.
Effects of Ablation on Hypersonic Aerodynamic Stability Characteristics. AIAA Paper 66-410, 1966.

3.31 Intrieri, Peter F.
Kirk, Donn B.
Terry, J.E.
Ablation Testing in Ballistic Ranges. AIAA Paper No.68-385, April 1968.

3.32 Intrieri, Peter F.
Kirk, Donn B.
Chapman, Gary T.
Ballistic Range Tests of Ablating and Nonablating Slender Cones. AIAA Paper 69-179, Jan. 1969.

3.33 Crogan, Leonard E.
Drag and Stability Data Obtained from Free-Flight Hypersonic Firings of Both Sharp and Blunt-Nosed 12-degree 40-Minute Total Angle Cones at Several Range Pressures. TR 63-36, NOL, 1966.

3.34 Intrieri, Peter F.
Experimental Stability and Drag of a Pointed and a Blunted 30° Half-Angle Cone at Mach Numbers from 11.5 to 34 in Air. NASA TN D-3193, 1966.

3.35 Compton, Dale L.
Cooper, David M.
Measurements of Radiative Heating on Sharp Cones. AIAA Journal, Vol.3, No.1, Jan. 1965, pp.107-114.

3.36 Denardo, B.Pat
Penetration of Polyethylene into a Semi-Infinite 2024-T351 Aluminium up to Velocities of 37,000 Feet per Second. NASA TN D-3369, 1966.

3.37 Collins, Daniel,J.
Sangster, David K.
Rogers, Walter K.
Feasibility Study on Small Particle Ablation Using a Free-Flight Range. CR-66-2128, General Motors DRS and Sandia Corp., Nov. 1966.

3.38 Timoshenko, S.
Goodier, J.H.
Theory of Elasticity. 2nd ed. McGraw-Hill, 1951, pp.416-421.

3.39 Curtis, John S.
Sabots. CTN64-04, General Motors DRL, Aug. 1964.

3.40 Wilkins, Max E.
Darsow, John F.
Finishing and Inspection of Model Surfaces for Boundary-Layer-Transition Tests. NASA Memo 1-19-59A, Feb. 1959.

3.41 Solnoky, P.
Some Recent Developments in Projectile Launching Techniques at Canadian Armament Research and Development Establishment. CARDE TM 727-62, Oct. 1962.

3.42 Teng, R.N.
Advances in Light-Gas Gun Model Launching Techniques. AIAA Journal Vol.5, No.11, Nov. 1967, pp.2082-2084.

TABLE 3.1

Physical Characteristics of Commonly used Materials

(Ref.: Materials in Design Engineering, Materials Selector Issue, Vol.60, No.5)

Material	*Density* *(g/cc)*	*Ultimate Strength*		*Strength/weight ratio*
		$\left(\frac{\text{newtons}}{m^2} \times 10^{-6}\right)$	$\left(\frac{\text{lbf}}{in^2} \times 10^{-3}\right)$	$\left(\frac{\text{newtons}}{m^2} \times 10^{-6}\right)$
Metals				
Tungsten	19.4	1520	(220)	78
Tantalum TA-10W	16.8	1100	(160)	65
Steel 4340	7.8	1980	(287)	254
Titanium 7Al-4Mo (Heat treat, max)	4.5	1380	(200)	307
Aluminum 7075 T6	2.8	572	(83)	204
Aluminum 2024 T3	2.8	483	(70)	172
Magnesium AZ63A	1.8	276	(40)	153
Plastics				
Fluorocarbon Teflon	2.2	45	(6)	20
Polycarbonate Lexan	1.2	65	(9)	54
Polyamides Nylon 66	1.1	83	(12)	75
Polyethylene High mol. wt.	0.94	37	(5)	39

TABLE 3.2

Model, Facility, and Test Requirements

Model	*10° half-angle cone*	
Test Conditions:	Mach number 15	
	Reynolds number (based on model diameter) from 100,000 to 1,000,000	
Facility:	instrumented length	23 meters
	shadowgraph stations	16 orthogonal pairs
	station spacing	1.5 meters
	pressure capability	1 atm to 0.001 atm
	air temperature	290°K
Gun:	1.27 cm diameter light gas gun (deformable-piston, isentropic-compression)	

TABLE 3.3

Model Characteristics

R_{e_∞} (based on d)	100,000	500,000	1,000,000
Model dia. (cm) Model material	0.84 Nylon	0.84 Aluminum	0.84 Steel
Weight (gram)	0.27	0.63	1.80
ρ_∞ (atm)	0.034	0.17	0.34
I_y ($kg\text{-}m^2$)	0.8×10^{-8}	1.8×10^{-8}	5.1×10^{-8}
X_D ($C_D = 0.10$) (cm)	6.9	14.7	10.4
λ (m)	12	8	10
Z_{swerve} (cm)	0.5	0.5	0.5

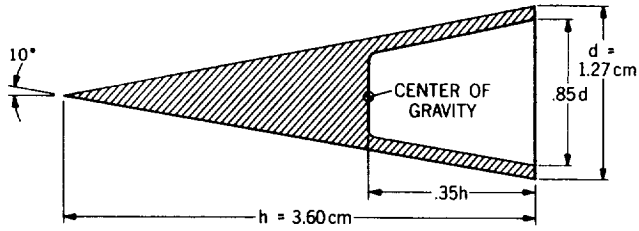

Fig. 3.1 Sketch of cone hollowed out for aerodynamic stability

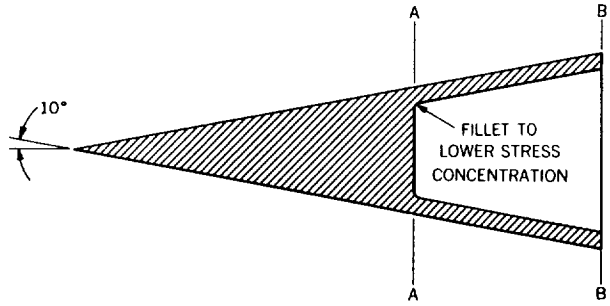

Fig. 3.2 Sketch of critical sections for stress analysis

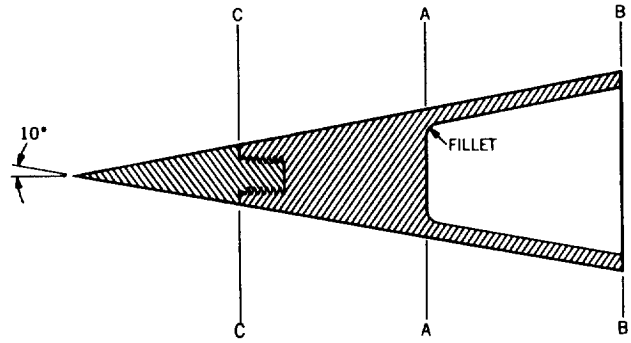

Fig. 3.3 Sketch of bimetallic hollow-base model

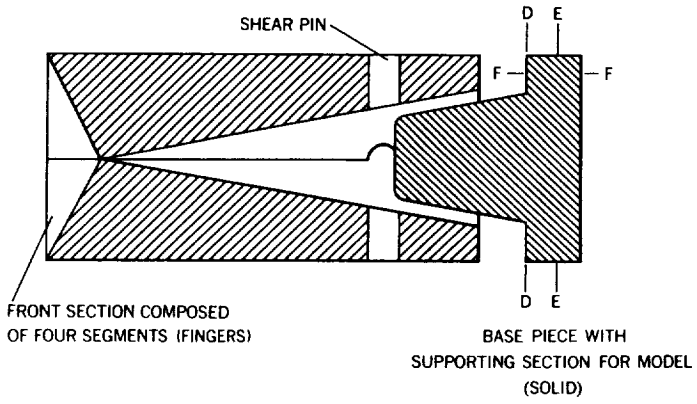

Fig. 3.4 Sketch of enclosing sabot for plastic cone model

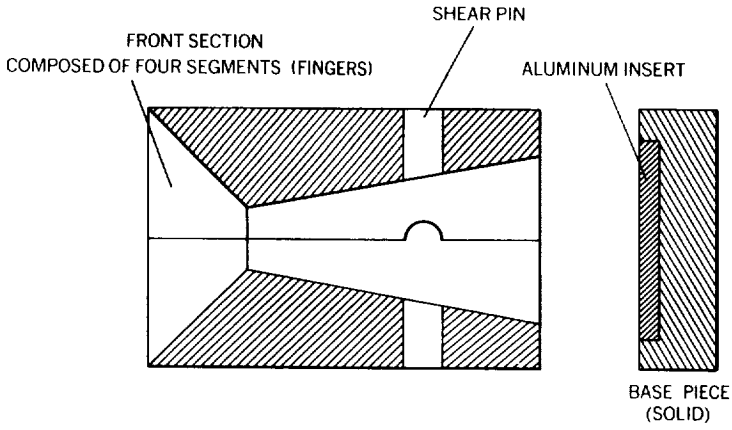

Fig. 3.5 Sketch of semi-enclosing sabot for metal cone model

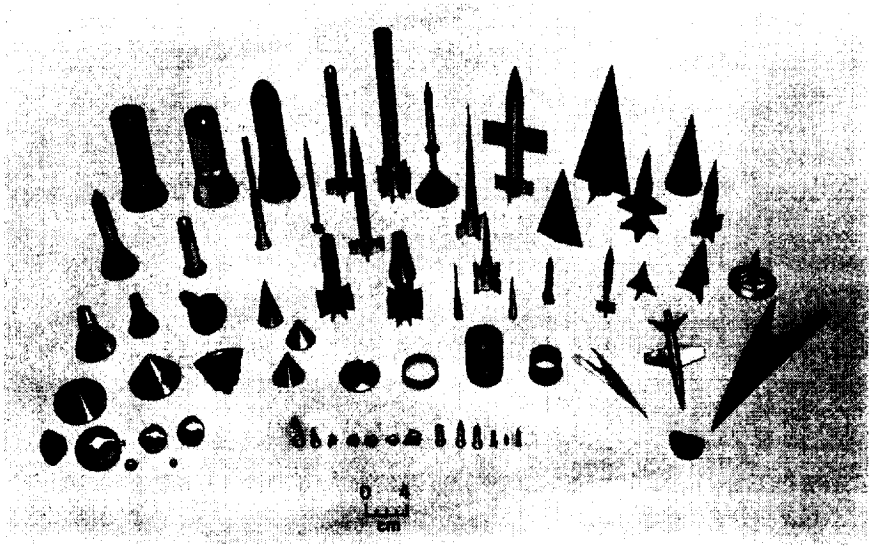

Fig. 3.6 Photograph showing variety of models tested at Hypersonic Free-Flight Branch, Ames Research Center

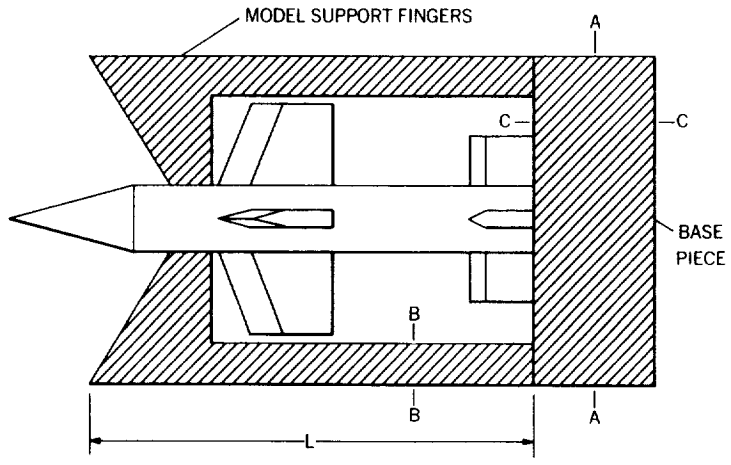

Fig. 3.7 Sketch of critical sections for stress analysis

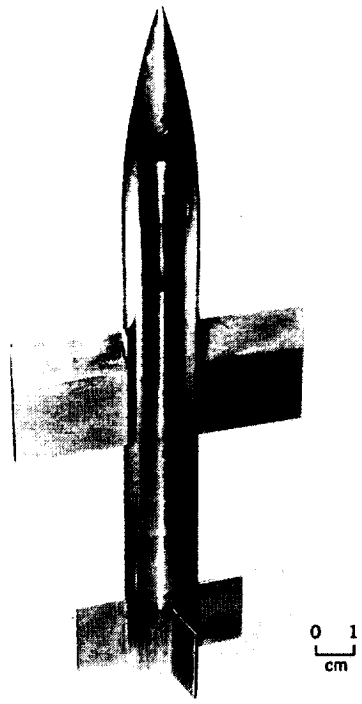

V_m, km/s	ρ, atm	GUN	REF
0.5	1.0	76mm POWDER GAS	3.2

Fig. 3.8 Photograph of airplane-type model

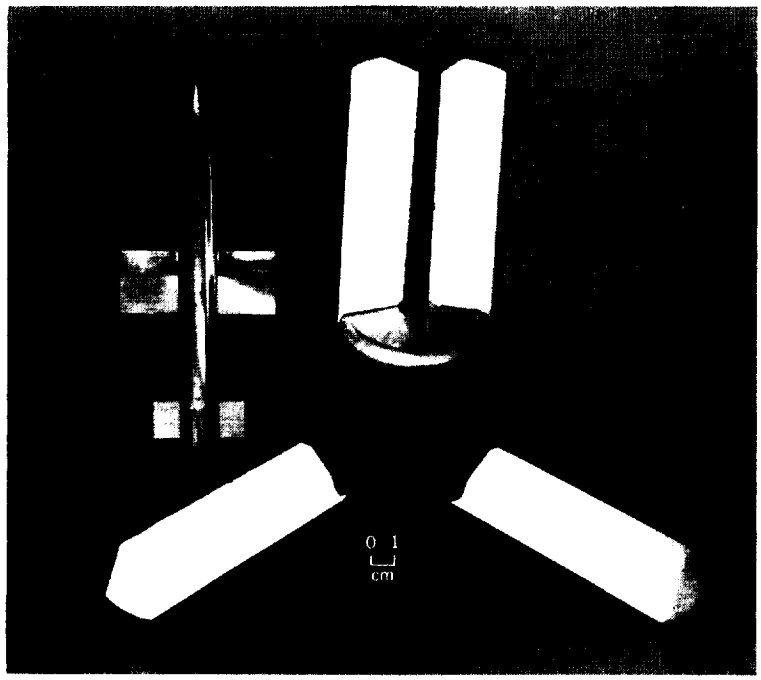

Fig. 3.9 Photograph of airplane-type model with sabot

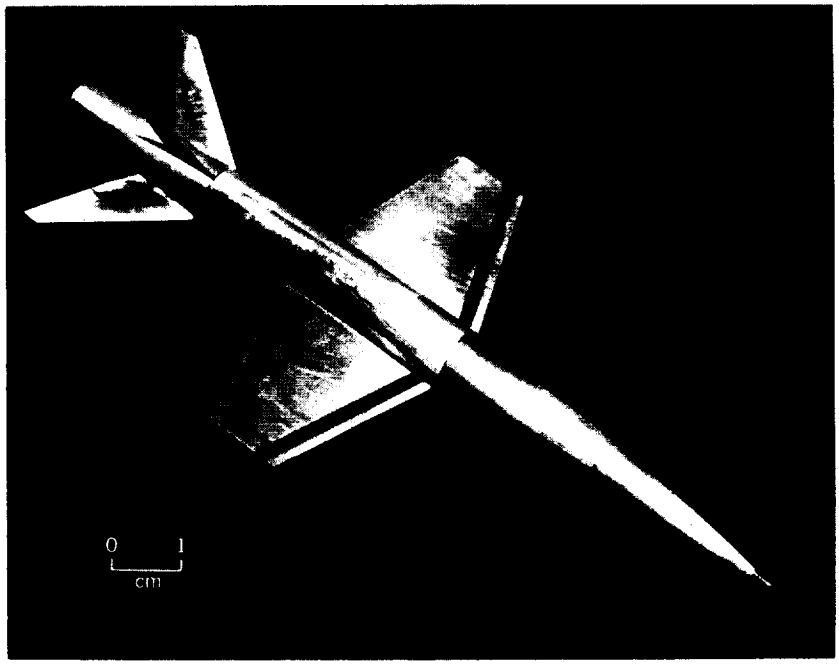

V_m, km/s	ρ, atm	GUN	REF
0.4	1.0	76 mm POWDER GAS	NONE (AMES)

Fig. 3. 10 Photograph of winged-body model

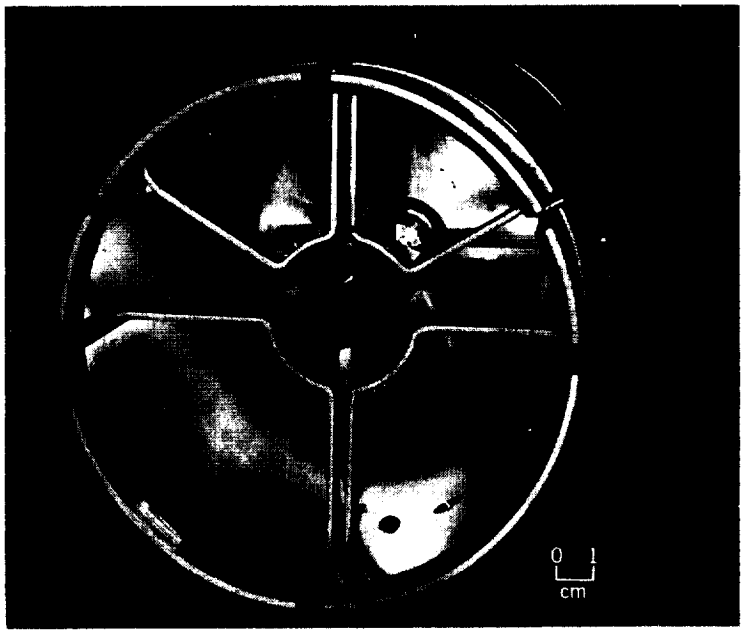

Fig. 3. 11 Cylindrical sabot for winged models. (Courtesy of Canadian Armament Research and Development Establishment.)

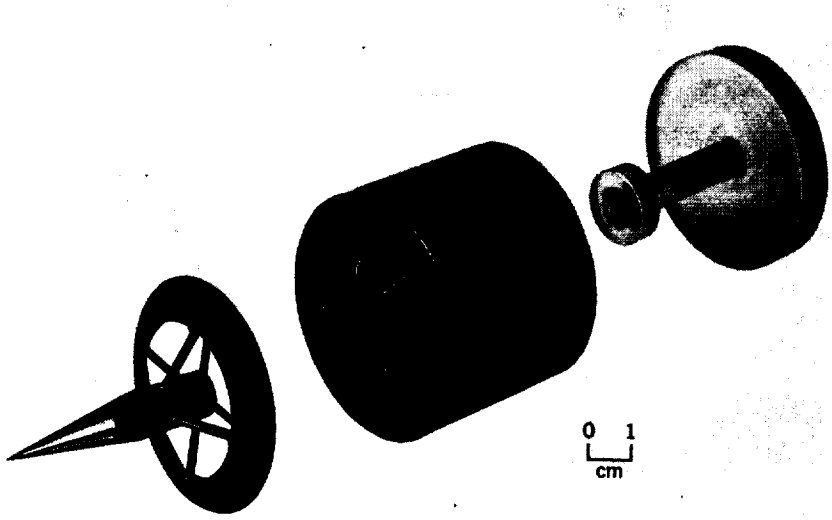

V_m, km/s	ρ, atm	GUN	REF
0.8	0.01	57 mm POWDER GAS	3.4

Fig. 3. 12 Photograph of Martin Mars-Probe model and sabot

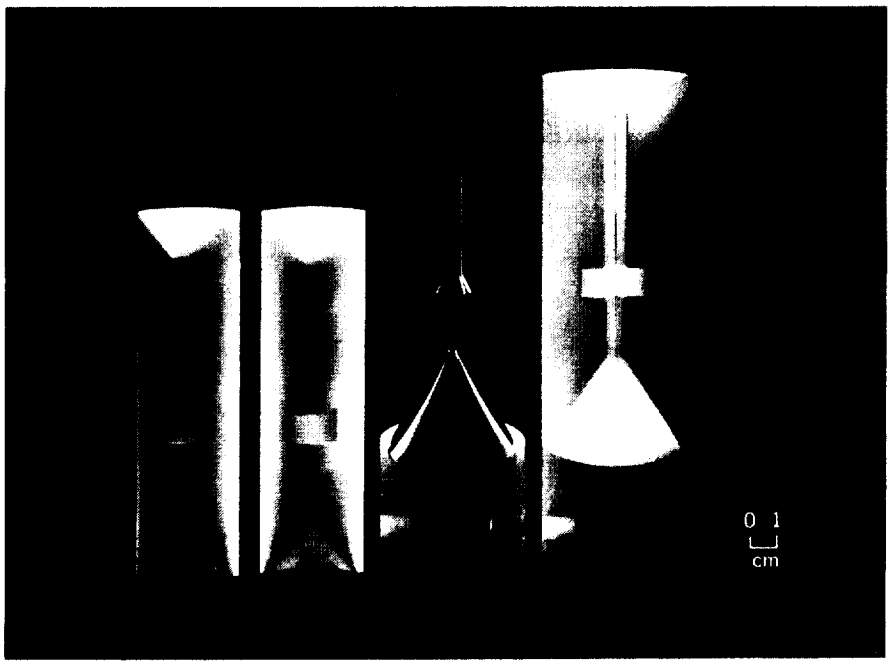

V_m, km/s	ρ, atm	GUN	REF
0.4	1.0	57 mm POWDER GAS	3.5

Fig. 3. 13 Photograph of Apollo launch-escape-configuration model and sabot

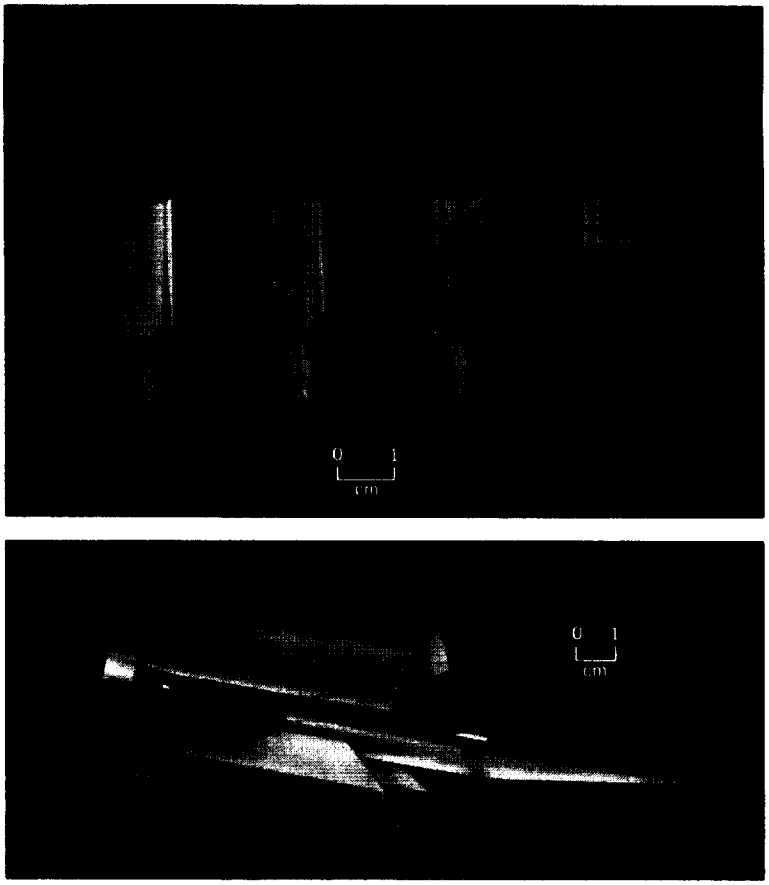

V_m, km/s	V_R, km/s	ρ, atm	GUN	REF
0.8	1.3	0.1-1.0	37 mm RIFLED POWDER GAS	3.6

Fig. 3. 14 Photograph of trailing-edge-spoiler models and model-sabot combination

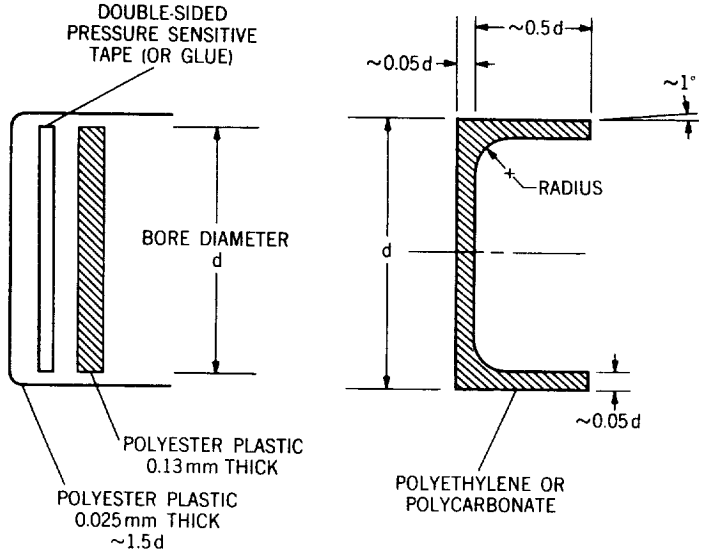

(a) Composite seal (b) Obturation cup

Fig. 3. 15 Sketch of two types of gas seals

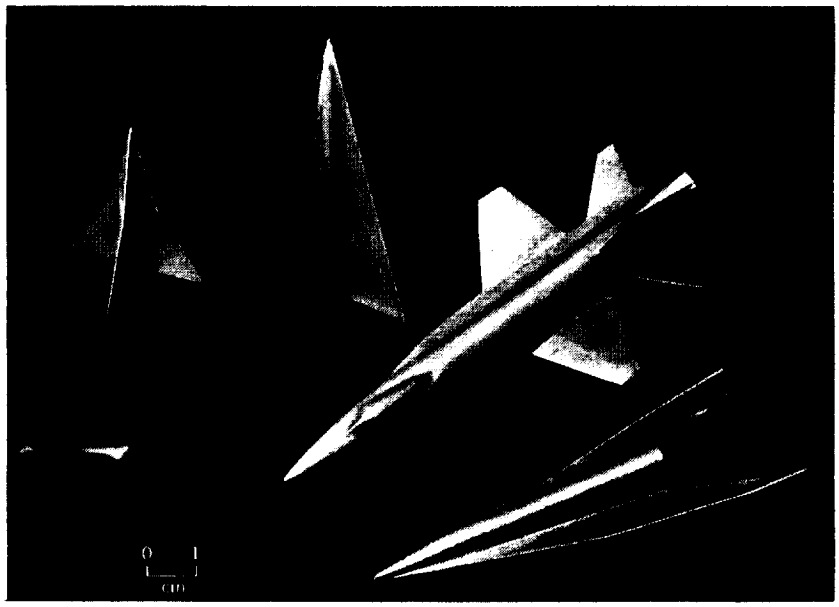

Fig. 3.16 Photograph of five investment-cast models

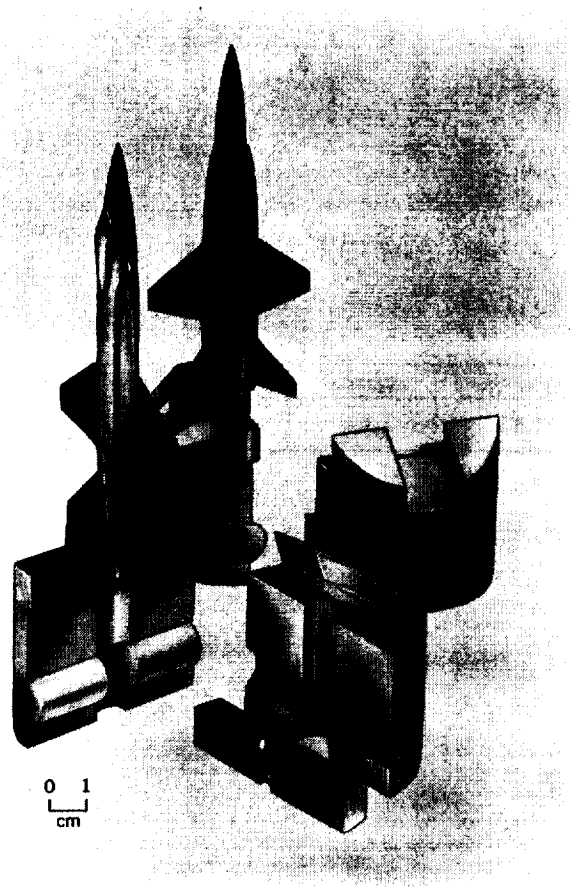

V_m, km/s	ρ, atm	GUN	REF
1.5	1.0	57 mm POWDER GAS	3.8

Fig. 3.17 Photograph of X-15 research-airplane model and sabot

V_m, km/s	V_R, km/s	ρ, atm	GUN	REF
1.3	1.8	0.1	57 mm POWDER GAS	3.9

Fig. 3.18 Photograph of three-wing-airplane model and sabot

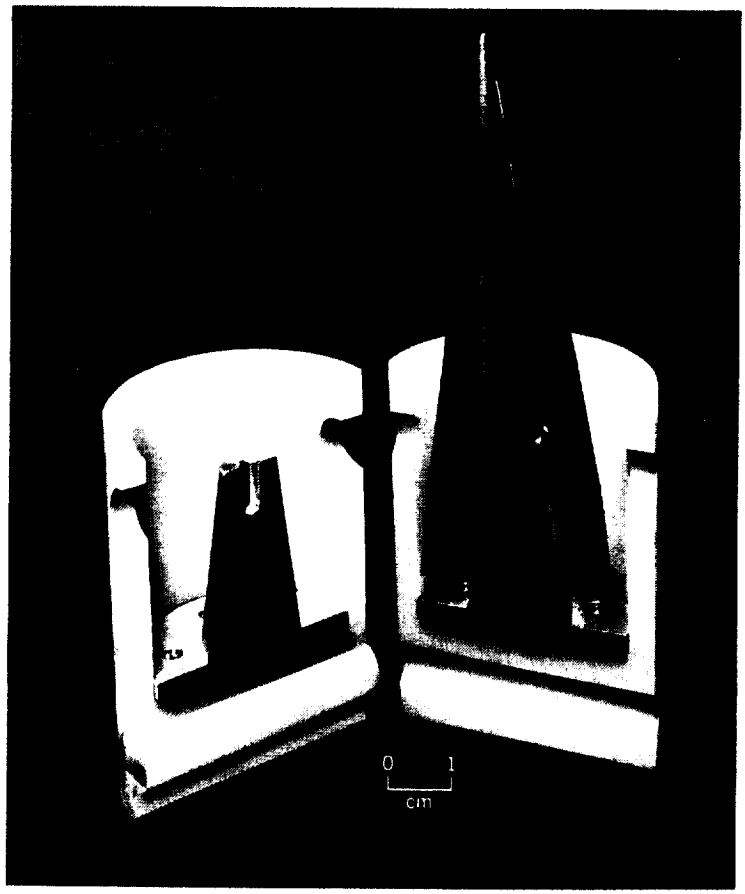

V_m, km/s	ρ, atm	GUN	REF
0.6	1.0	45 mm POWDER GAS	NONE (AMES)

Fig. 3. 19 Photograph of hypersonic-glider model and sabot

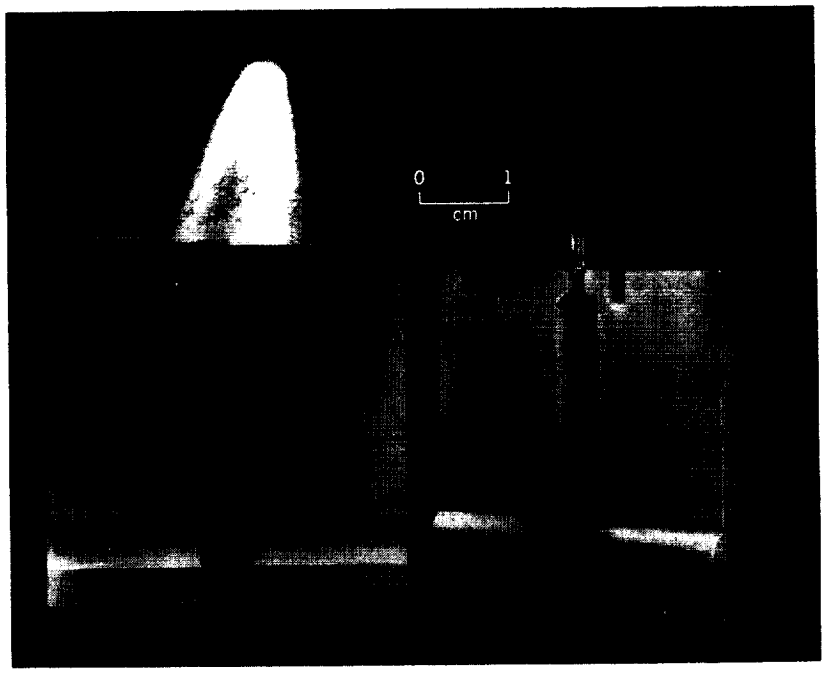

V_m, km/s	ρ, atm	GUN	REF
1.1	0.07	45 mm POWDER GAS	3.11

Fig. 3. 20 Photograph of half-cone lifting-body model and sabot

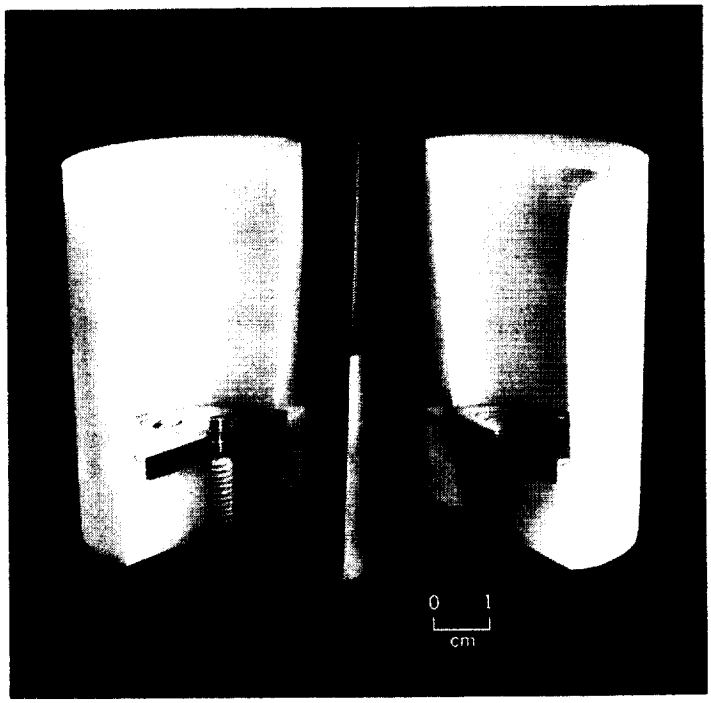

V_m, km/s	ρ, atm	GUN	REF
1.4	1.0	57 mm POWDER GAS	3.12

Fig. 3. 21 Photograph of 74°-swept-back delta-wing model and sabot

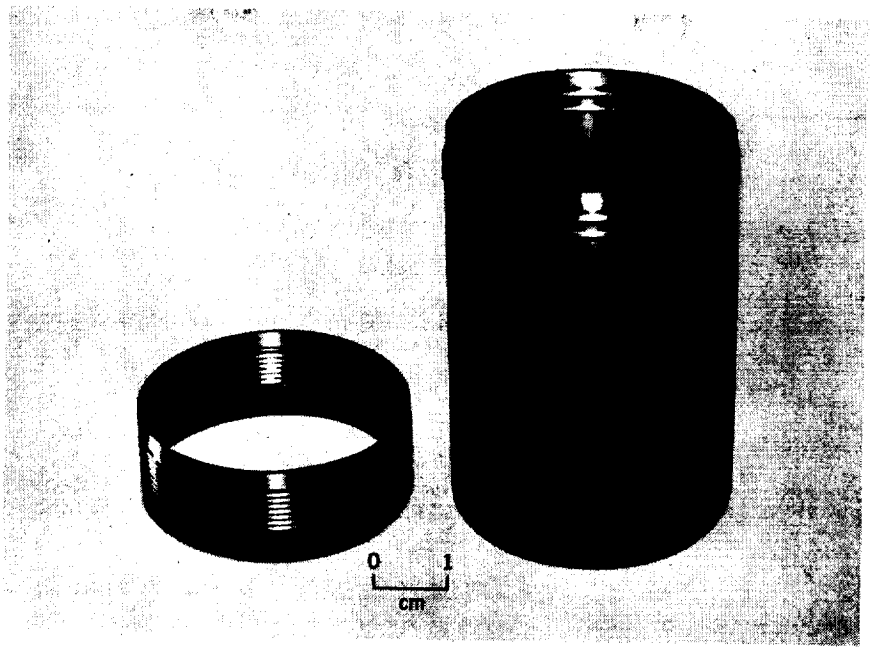

V_m, km/s	V_R, km/s	ρ, atm	GUN	REF
1.3	1.8	1.0	37 mm RIFLED POWDER GAS	3.13

(a) Photograph of skin-friction-drag models

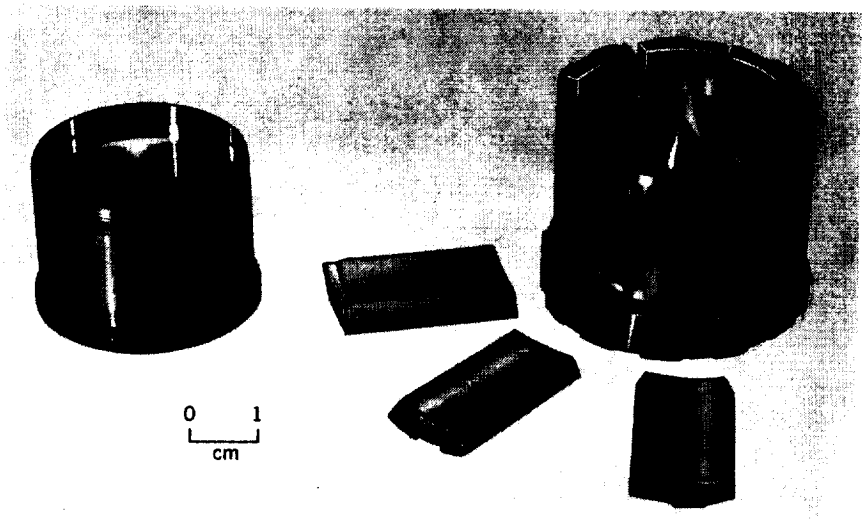

V_m, km/s	V_R, km/s	ρ, atm	GUN	REF
0.8	1.3	0.1-1.0	37 mm RIFLED POWDER GAS	3.6

(b) Photograph of spoiler-drag models

Fig. 3.22 Photograph of two varieties of open-ended-tube models

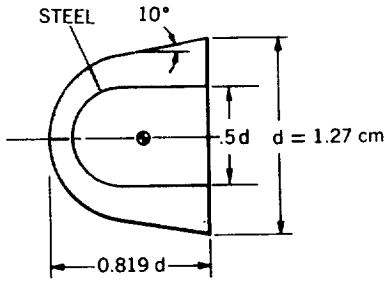

(a) Sketch of model

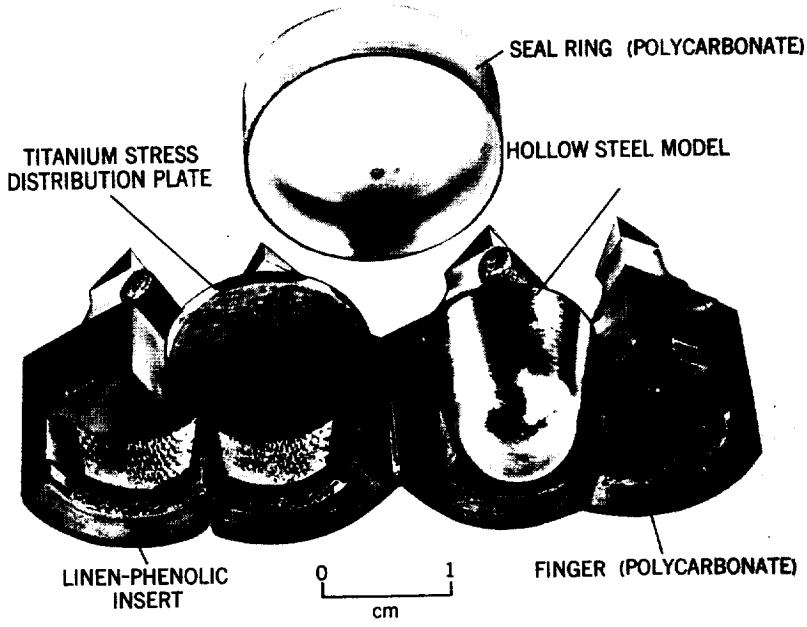

(b) Photograph of model with sabot

V_m, km/s	ρ, atm	GUN	REF
4.7	.12	20 mm TWO-STAGE LIGHT GAS	3.16, 3.17

Fig. 3.23 Short blunt cone, hollow base. (Courtesy of Jet Propulsion Laboratory and US Naval Ordnance Laboratory.)

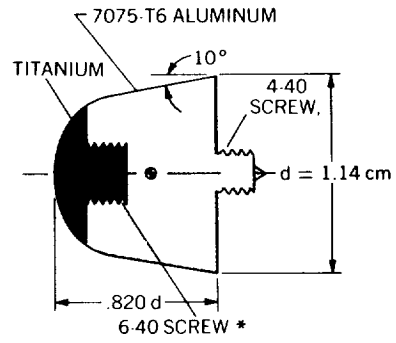

(a) Sketch of model

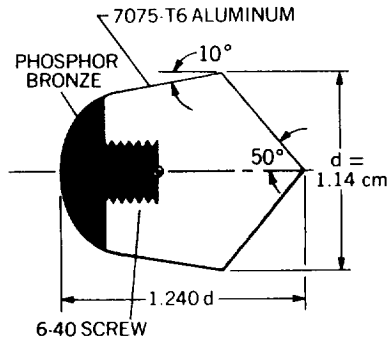

(b) Sketch of model with afterbody

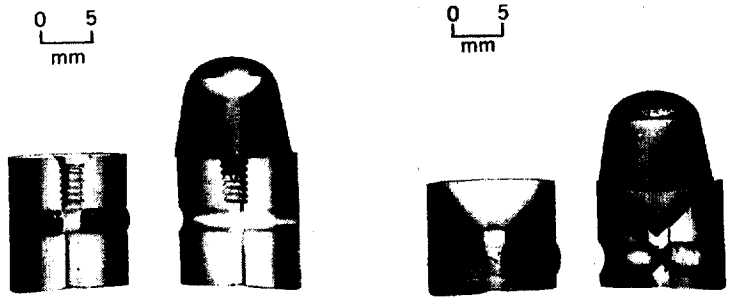

(c) Photographs of models with sabots

* SCREW THREADS DESIGNATED IN THIS CHAPTER ARE AMERICAN STANDARD FINE-THREAD SERIES.

V_m, km/s	ρ, atm	GUN	REF
3.0	.1	12.7 mm SINGLE-STAGE LIGHT GAS	3.18, 3.19

Fig. 3. 24 Short blunt cone (ballasted)

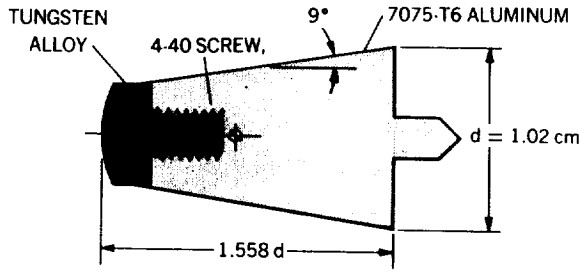

(a) Sketch of model

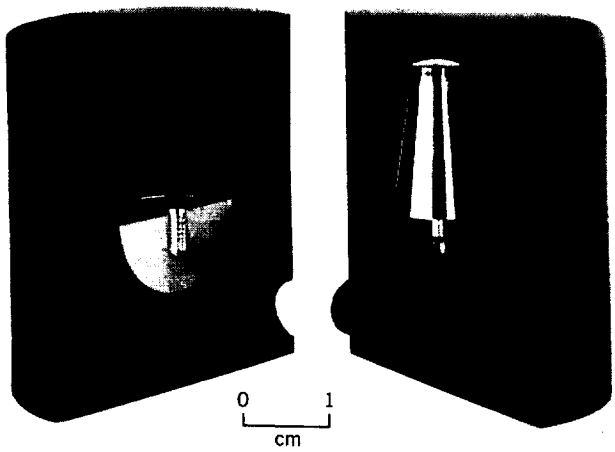

(b) Photograph of model with sabot

V_m, km/s	V_R, km/s	ρ, atm	GUN	REF
3.0	3.7	.38	37 mm SINGLE-STAGE LIGHT GAS	3.20

Fig. 3.25 Blunt-nosed 9^{o} cone

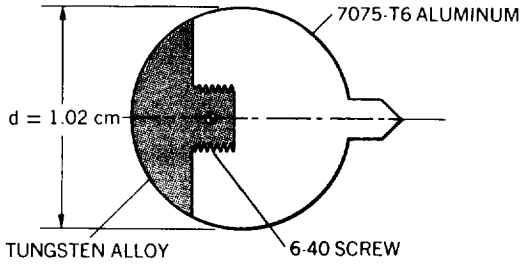

(a) Sketch of model

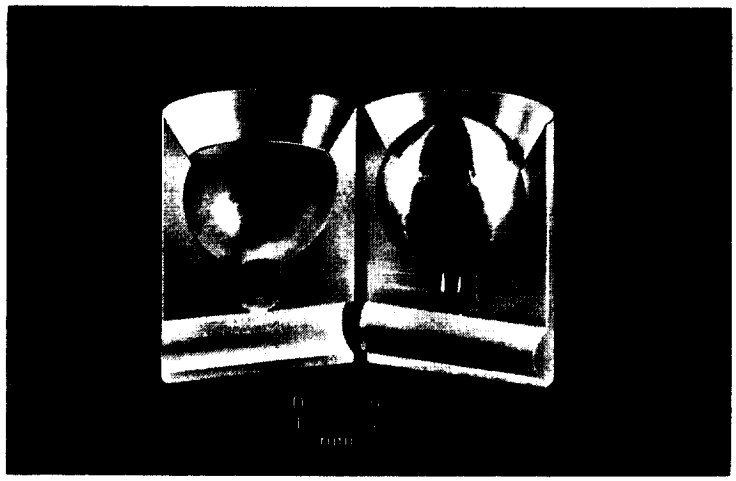

(b) Photograph of model with sabot

V_m, km/s	ρ, atm	GUN	REF
5.0	.25	12.7 mm DEFORMABLE-PISTON LIGHT GAS	3.21
4.0	1.0		

Fig. 3.26 Ballasted sphere

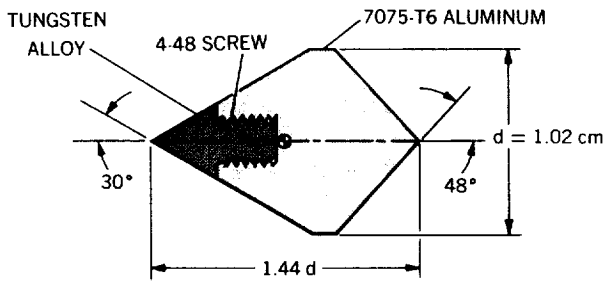

(a) Sketch of model

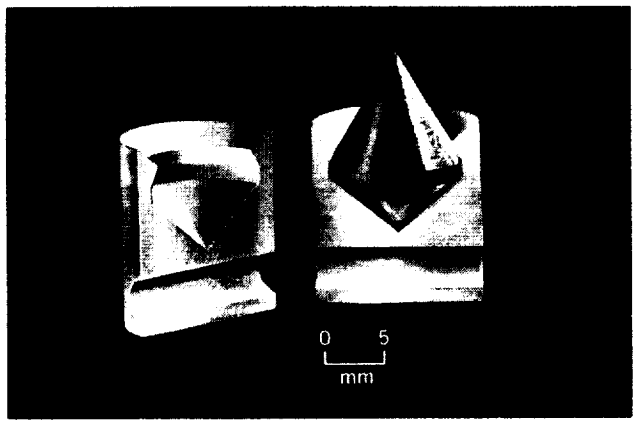

(b) Photograph of model with sabot

V_m, km/s	ρ, atm	GUN	REF
3.0	.4	12.7 mm DEFORMABLE-PISTON LIGHT GAS	3.23

Fig. 3.27 Conical body

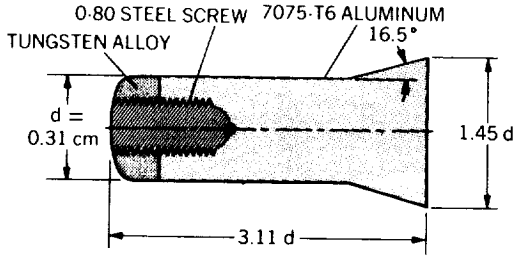

(a) Sketch of model

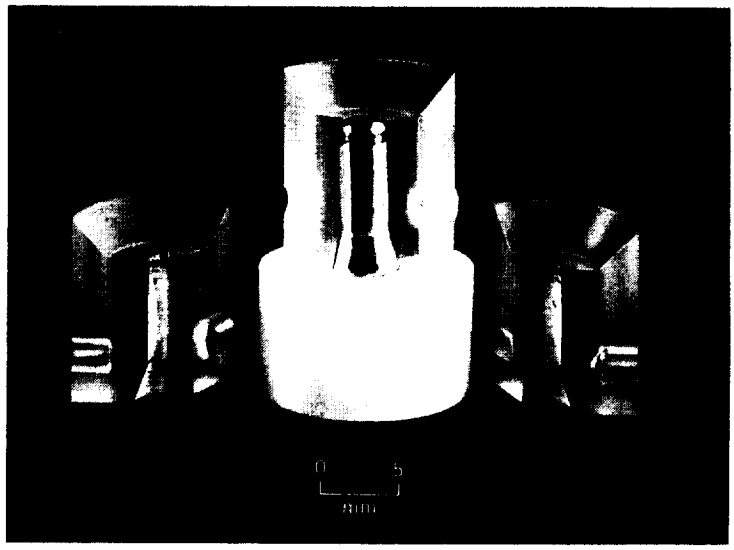

(b) Photograph of model with sabot

V_m, km/s	V_R, km/s	ρ, atm	GUN	
6.4	8.2	.03	12.7 mm DEFORMABLE-PISTON LIGHT GAS	3.24

Fig. 3.28 Blunt-nosed flare-stabilized body

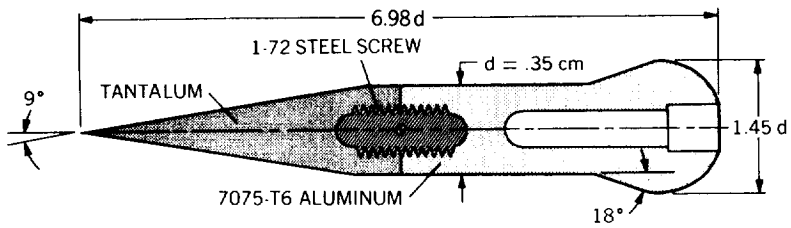

(a) Sketch of model

(b) Photograph of models with sabots

V_m, km/s	V_R, km/s	ρ, atm	GUN	REF
3.8	5.7	.12	12.7 mm DEFORMABLE-PISTON LIGHT GAS	3.25

Fig. 3.29 Sharp-nosed flare-stabilized body

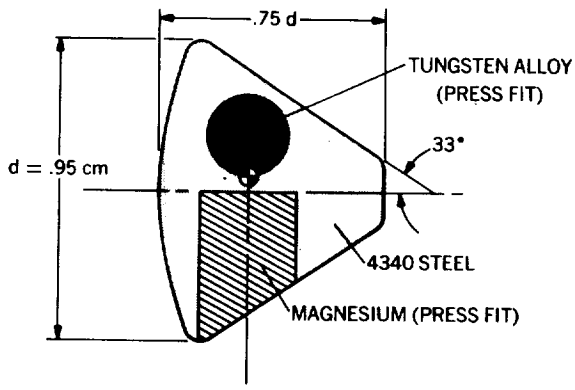

(a) Sketch of model

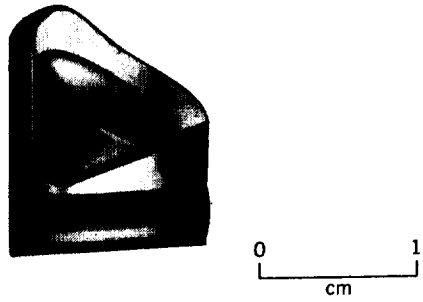

(b) Photograph of model with sabot

V_m, km/s	V_R, km/s	ρ, atm	GUN	REF
4.9	—	.1	12.7 mm DEFORMABLE-PISTON LIGHT GAS	3.26
4.9	7.6	.02		

Fig. 3.30 Apollo-type body

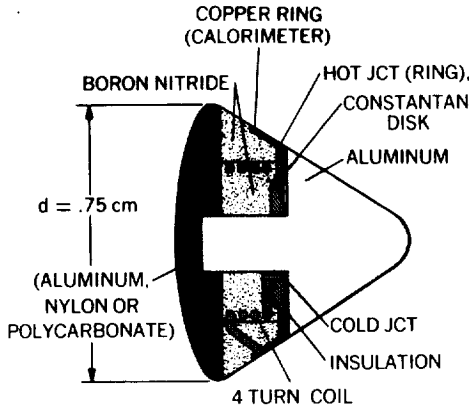

(a) Sketch of model

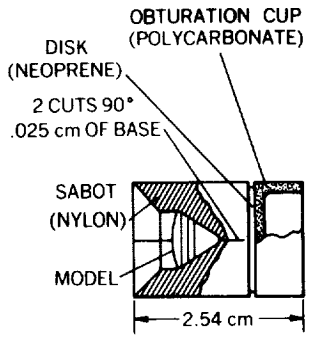

(b) Sketch of model with sabot

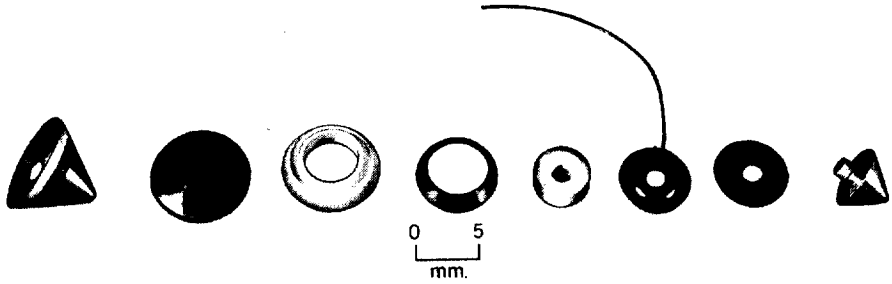

(c) Photograph of model components and assembled model

V_m, km/s	ρ, atm	GUN	REF
6.1	.13	15.2 mm DEFORMABLE-PISTON LIGHT GAS	3.27

Fig. 3.31 Passive-telemetry model

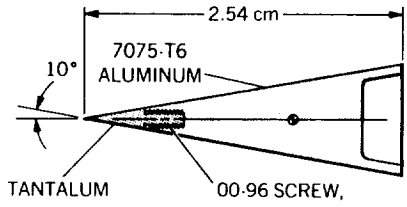

(a) Sketch of model

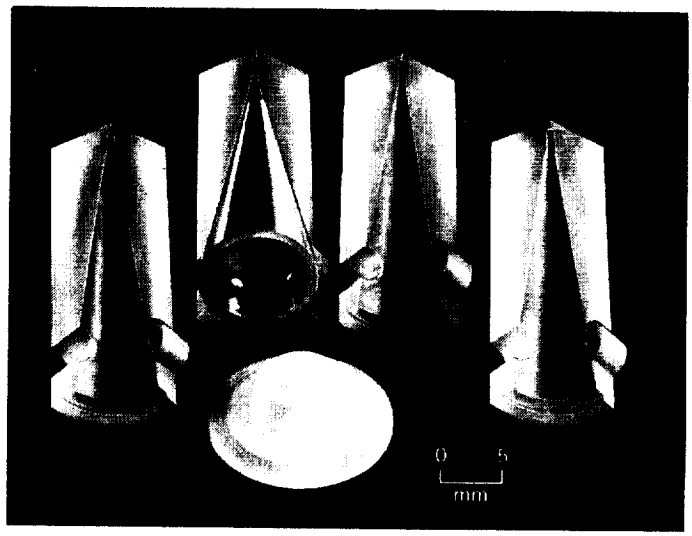

(b) Photograph of model with sabot

V_m, km/s	ρ, atm	GUN	REF
5.7	.04	12.7mm DEFORMABLE-PISTON LIGHT GAS	3.31, 3.32

Fig. 3.32 Sharp-nosed 10^o cone

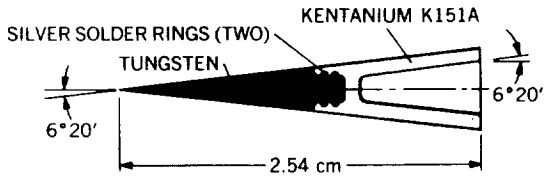

(a) Sketch of model

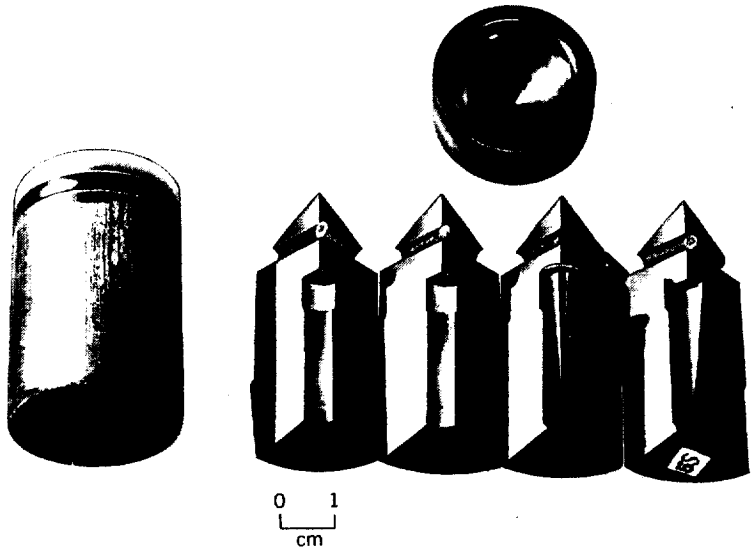

(b) Photograph of model with sabot

V_m, km/s	ρ, atm	GUN	REF
3.0	1	31.7 mm SINGLE-STAGE LIGHT GAS	3.33

Fig. 3.33 Sharp-nosed 6° 20′ cone. (Courtesy of US Naval Ordnance Laboratory.)

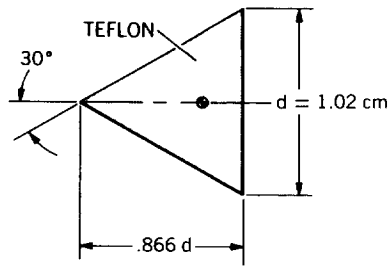

(a) Sketch of model

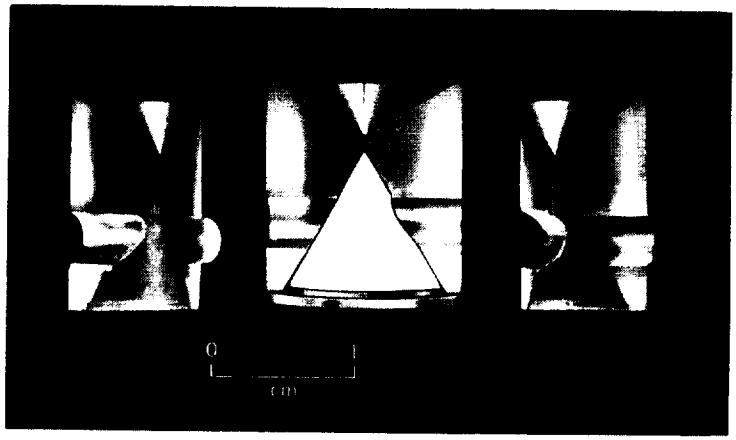

(b) Photograph of model with sabot

V_m, km/s	V_R, km/s	ρ, atm	GUN	REF
7.0	8.8	.02	12.7 mm DEFORMABLE-PISTON LIGHT GAS	3.34

Fig. 3.34 30° Teflon cone

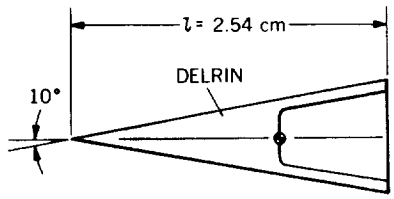

(a) Sketch of model

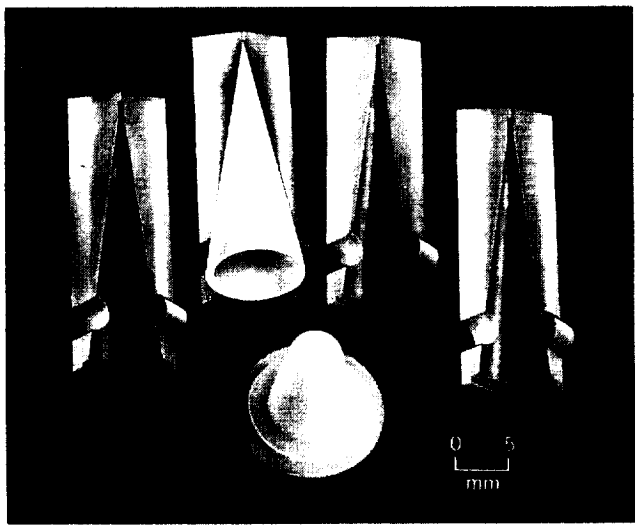

(b) Photograph of model with sabot

V_m, km/s	ρ, atm	GUN	REF
5.7	.04	12.7 mm DEFORMABLE-PISTON LIGHT GAS	3.31, 3.32

Fig. 3.35 10^{o} Delrin cone

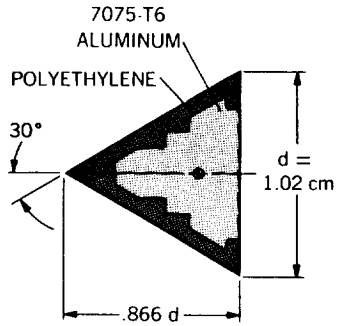

(a) Sketch of model

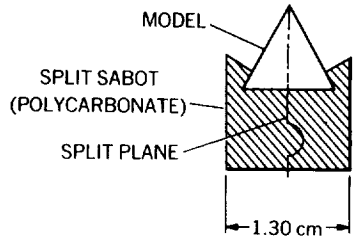

(b) Sketch of model with sabot

V_m, km/s	ρ, atm	GUN	REF
7.3	.026	12.7 mm DEFORMABLE-PISTON LIGHT GAS	3.35

Fig. 3.36 30° cone with injection-molded plastic shell

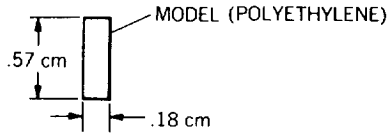

$MASS_{MODEL}$ = .0453 gm
V_{MODEL} = 11.3 km/s
P = 1.20 mmHg
GUN = 22 CALIBER
DEFORMABLE PISTON
LIGHT GAS
(SMOOTH BORE)
REF = 3.36

Fig. 3.38 Sketch of thin right-circular-cylinder model.

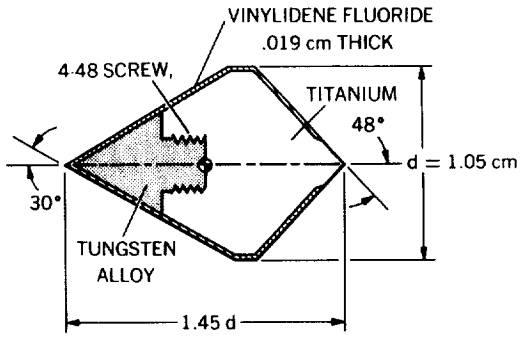

(a) Sketch of model

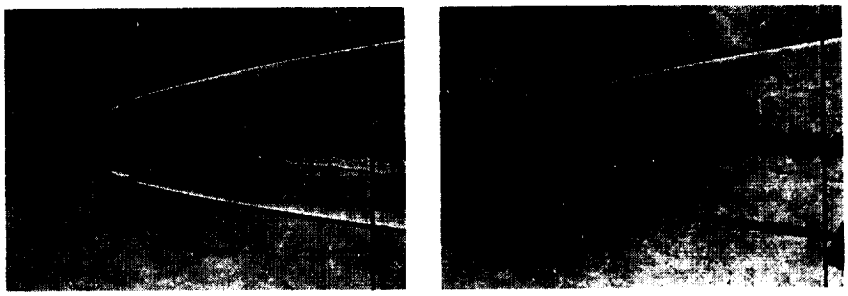

First station (x = 0) Last station (x = 12.2 m)

(b) Shadowgraphs showing negligible tip blunting

V_m, km/s	ρ, atm	GUN	REF
4.6	.4	12.7 mm DEFORMABLE-PISTON LIGHT GAS	3.23

Fig. 3.37 Conical body with thin plastic coating

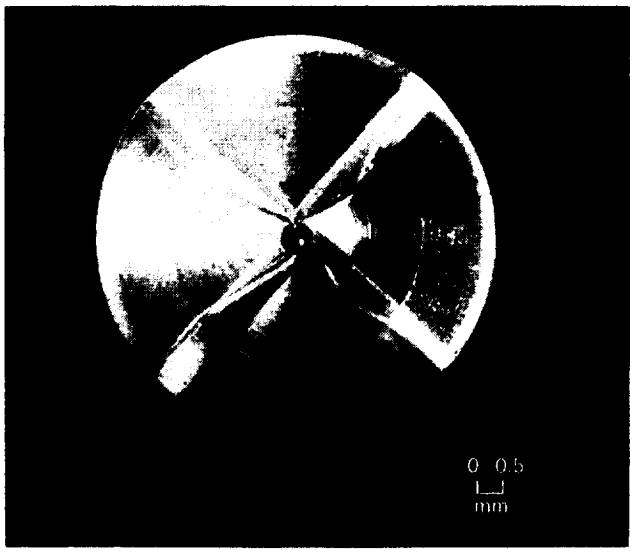

(a) Front view of sabot with model

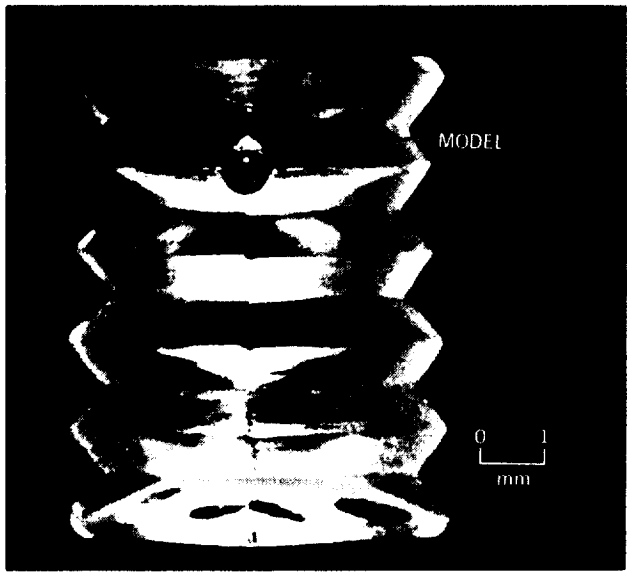

(b) Segmented view of sabot with model

V_m, km/s	ρ, atm	GUN	REF
8	.03	7.6 mm TWO-STAGE LIGHT GAS	3.3

Fig. 3.39 Photographs of model (700-micron Al_2O_3 sphere) with serrated sabot. (Courtesy of General Motors Defense Research Laboratories.)

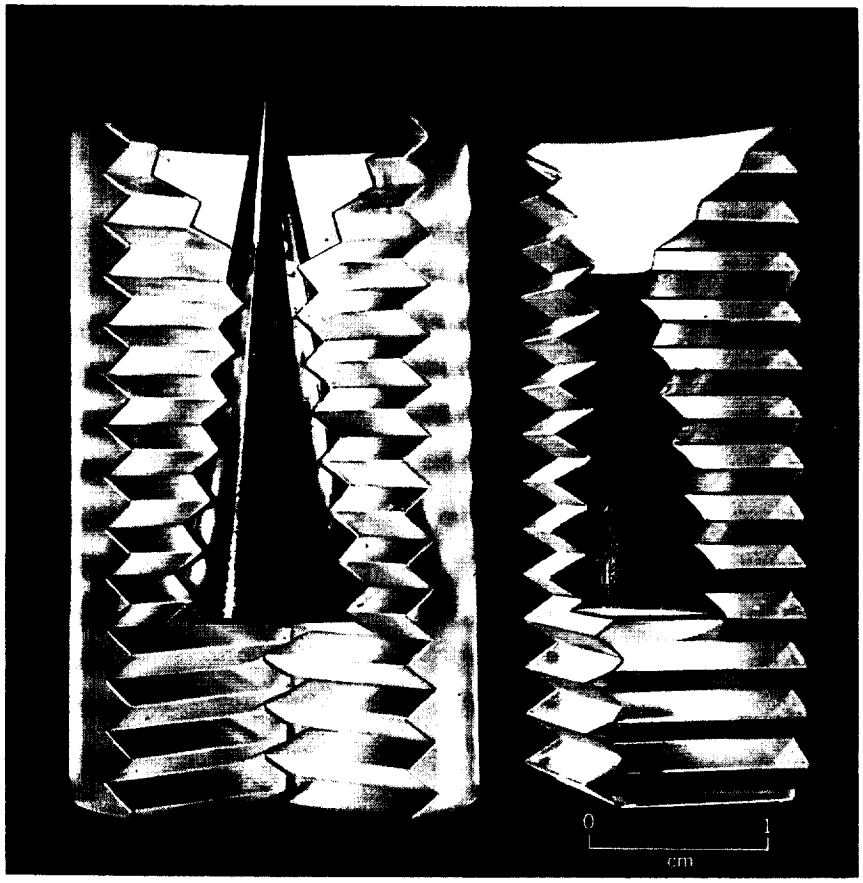

Fig.3.40 Photograph of cone model with serrated sabot. (Courtesy of General Motors Defense Research Laboratories.)

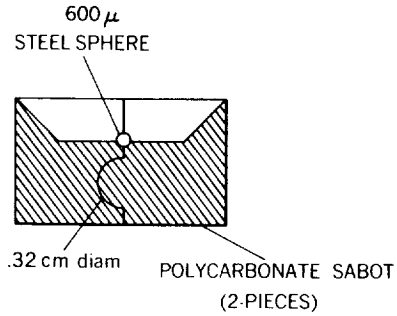

$d_{MODEL} = 600\,\mu$
$MASS_{MODEL} = .001$ g
$MASS_{SABOT} = .980$ g
$d_{SABOT} = 1.31$ cm
$l_{SABOT} = .81$ cm
$V_{MODEL} = 8.3$ km/s
P = .05 atm
GUN = 50 CALIBER DPLG*
REF = NONE (AMES)

* DEFORMABLE-PISTON LIGHT GAS

Fig.3.41 Sketch of sabot for 600-micron steel sphere

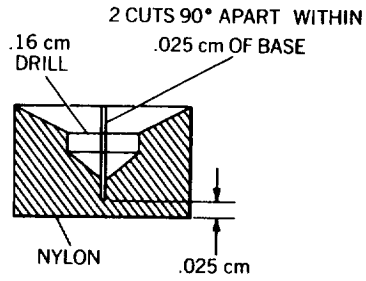

d_{MODEL} = .16 cm
$MASS_{MODEL}$ = .0060 g
$MASS_{SABOT}$ = .080 g
d_{SABOT} = .54 cm
l_{SABOT} = .33 cm
V_{MODEL} = 9.4 km/s
P = 28 mmHg
GUN = 22 CALIBER DPLG* (SMOOTH BORE)
REF = NONE (AMES)

Fig. 3.42 Sketch of sabot for 1600-micron aluminum sphere.

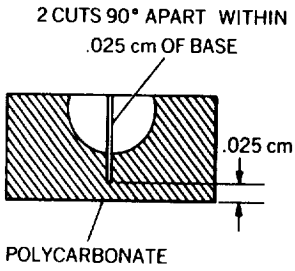

d_{MODEL} = .32 cm
$MASS_{MODEL}$ = .0374 g
$MASS_{SABOT}$ = .0875 g
d_{SABOT} = .57 cm
l_{SABOT} = .28 cm
V_{MODEL} = 8.8 km/s
P = 1-6 mmHg
GUN = 22 CALIBER DPLG* (RIFLED)
REF = NONE (AMES)

Fig. 3.43 Sketch of sabot for 3200-micron Pyrex-glass sphere

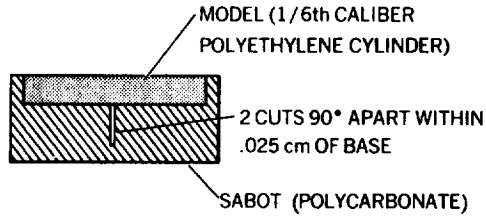

l_{MODEL} = .08 cm
d_{MODEL} = .51 cm
$MASS_{MODEL}$ = .0161 g
$MASS_{SABOT}$ = .0595 g
d_{SABOT} = .58 cm
l_{SABOT} = .25 cm
V_{MODEL} = 9.8 km/s
P = 1.70 mmHg
GUN = 22 CALIBER DPLG* (RIFLED)
REF = NONE (AMES)

Fig. 3.44 Sketch of thin cylinder model with sabot

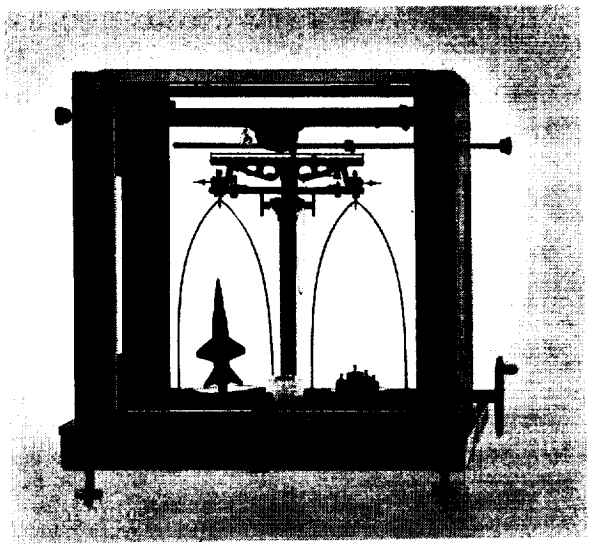

(a) Equal-arm type

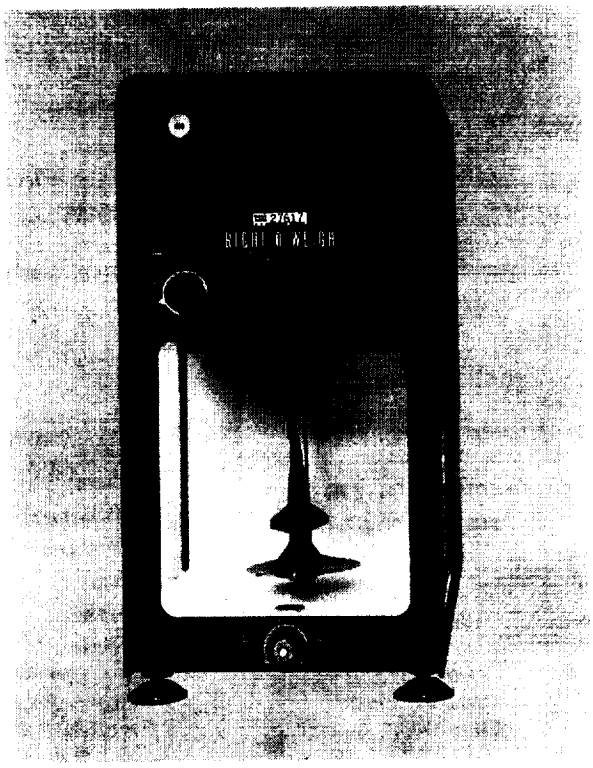

(b) Substitution type.

Fig.3.45 Two types of analytical balances for measuring model mass.

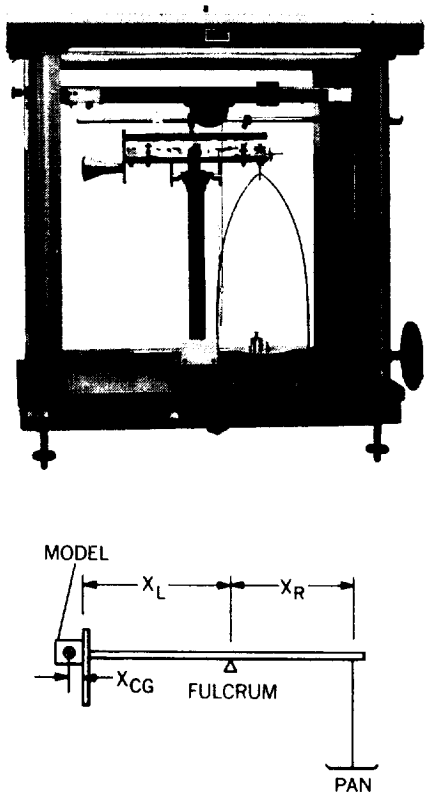

Fig. 3.46 Equipment for the determination of model center of gravity

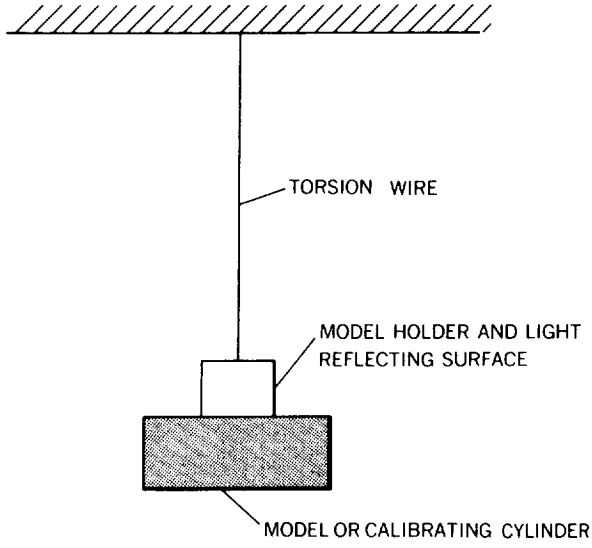

Fig. 3.47 Sketch of torsion-pendulum setup for moment-of-inertia measurements

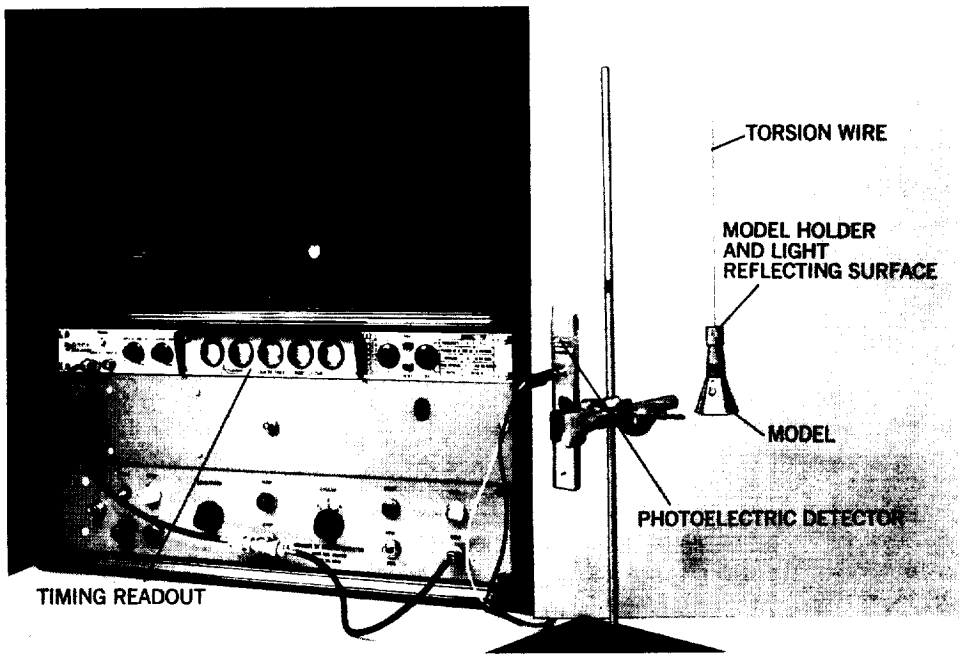

Fig.3.48 Photograph of moment-of-inertia apparatus

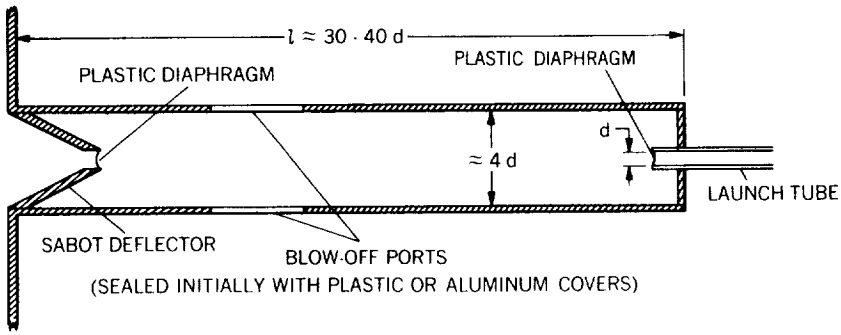

Fig.3.49 Sketch of simple sabot-separating tank

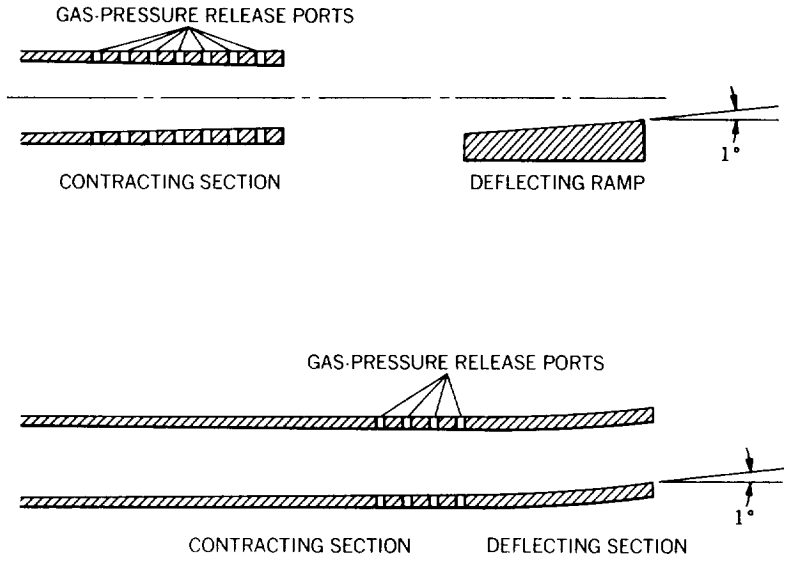

Fig.3.50 Sketch of two types of sabot decelerators and deflectors

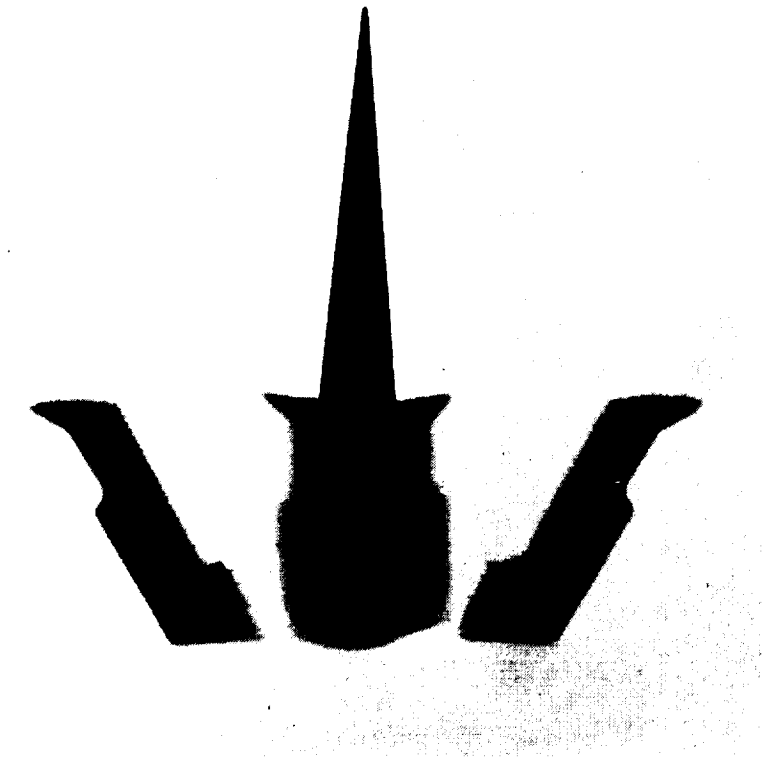

Fig.3.51 X-ray shadowgram showing separation of sabot from model. (Courtesy of von Kármán Gas Dynamics Facility, Arnold Engineering Development Center.)